Microbial Cell Factories

RESEARCH

Open Access

Unveiling the potential of novel *Metschnikowia* yeast biosurfactants: triggering oxidative stress for promising antifungal and anticancer activity

Sumeeta Kumari[1†], Alka Kumari[1†], Asmita Dhiman[1], Kanti Nandan Mihooliya[1], Manoj Raje[1], G. S. Prasad[1] and Anil Kumar Pinnaka[1*]

Abstract

Background Sophorolipids are glycolipid biosurfactants with potential antibacterial, antifungal, and anticancer applications, rendering them promising for research. Therefore, this study hypothesizes that sophorolipids may have a notable impact on disrupting membrane integrity and triggering the production of reactive oxygen species, ultimately resulting in the eradication of pathogenic microbes.

Results The current study resulted in the isolation of two *Metschnikowia* novel yeast strains. Sophorolipids production from these strains reached maximum yields of 23.24 g/l and 21.75 g/l, respectively, at the bioreactors level. Biosurfactants sophorolipids were characterized using FTIR and LC–MS techniques and found to be a mixture of acidic and lactonic forms with molecular weights of *m/z* 678 and 700. Our research elucidated sophorolipids' mechanism in disrupting bacterial and fungal membranes through ROS generation, confirmed by transmission electron microscopy and FACS analysis. The results showed that these compounds disrupted the membrane integrity and induced ROS production, leading to cell death in *Klebsiella pneumoniae* and *Fusarium solani*. In addition, the anticancer properties of sophorolipids were investigated on the A549 lung cancer cell line and found that sophorolipid-11D (SL-11D) and sophorolipid-11X (SL-11X) disrupted the actin cytoskeleton, as evidenced by immunofluorescence microscopy. The A549 cells were stained with Acridine orange/Ethidium bromide, which showed that they underwent necrosis. This was confirmed by flow cytometric analysis using Annexin/PI staining. The SL-11D and SL-11X molecules exhibited low levels of haemolytic activity and in-vitro cytotoxicity in HEK293, Caco-2, and L929 cell lines.

Conclusion In this work, novel yeast species CIG-11D^{T} and CIG-11X^{T}, isolated from the bee's gut, produce significant yields of sophorolipids without needing secondary oil sources, indicating a more economical production method. Our research shows that sophorolipids disrupt bacterial and fungal membranes via ROS production. They suggest they may act as chemo-preventive agents by inducing apoptosis in lung cancer cells, offering the potential for enhancing anticancer therapies.

[†]Sumeeta Kumari and Alka Kumari contributed equally to this work.

*Correspondence:
Anil Kumar Pinnaka
apinnaka@imtech.res.in
Full list of author information is available at the end of the article

Keywords *Metschnikowia*, Sophorolipids, Reactive oxygen species, Antifungal, Anticancer

Introduction

Sophorolipids are glycolipid biosurfactants produced by various yeast species, including *Starmerella bombicola*, *Rhodotorula babjevae, Candida apicola,* and *R. bogoriansis* [1–3]. These compounds have a hydrophilic carbohydrate head and a hydrophobic fatty acid tail, giving them surface-active properties. Sophorolipids are known for their biocompatibility, low toxicity, and biodegradability, making them an attractive alternative to synthetic surfactants in various industrial applications [4, 5]. Recently, they have gained attention for their potential as antimicrobial and anticancer agents [6]. They have been found to possess antimicrobial activity against several pathogenic microorganisms, including bacteria, fungi, and viruses, by destabilizing the membrane and increasing permeabilization [2, 3]. They have also been reported to exhibit inhibition against HIV and have shown anticancer activity [2].

Fungal infections are a significant global health problem. Over the past few decades, there has been a substantial increase in both community-acquired and nosocomial fungal infections. The risk of fungal infections has increased in patients suffering from immunosuppressed or immunodeficient conditions, and restricted therapeutic options are being made available, emphasizing the search for novel alternatives. Unfortunately, only three classes of potent antifungal agents-azoles, echinocandins, and polyenes, are available, and their limited spectrum and widespread use led to the development of drug-resistance strains of *Aspergillus*, *Candida*, *Fusarium*, and *Cryptococcus* [7]. Moreover, antifungal drugs currently used for the treatment have their limitations, such as severe toxicity, adverse side effects, and high costs of the existing antifungal agents [8]. Therefore, it is crucial to introduce new therapeutic agents that will maximize the potency and prevent drug resistance caused by pathogens. Sophorolipids have attributed several benefits, such as low toxicity, surface and interface activity, biocompatibility and digestibility, specificity and efficiency, and environmental remediation [9]. Sophorolipids have demonstrated promising antifungal activity against pathogenic fungi, including *Candida albicans*, *Aspergillus fumigatus*, and *Cryptococcus neoformans.* The mechanism of action of sophorolipids involves disruption of the fungal cell membrane, leading to leakage of intracellular contents and, ultimately, cell death [2, 3]. However, the antifungal activity of SLs has not been as extensively studied as their other applications and still requires investigation for novel yeast species with good productivity and broad applications.

Recently, biosurfactants have gained attention as a potential cancer chemotherapeutic drug due to their unique structures and biophysical properties [6]. Cancer is a leading cause of mortality worldwide, and the complexity of its etiology and the emergence of drug resistance make finding new anticancer drugs a challenging task [6]. The existing anticancer agents also hamper the treatment because of their toxicity, narrow therapeutic index, non-specific targeting, high cost, side effects, and limited efficacy in the advanced stage [10]. According to recent studies into potential pharmaceutical applications, sophorolipids may serve as anticancer therapeutics as they disrupt cell cycle progression and cause necrosis or apoptosis in a variety of cancerous cell lines, including cervical cancer [11], breast cancer [12, 13], and lung cancer [12]. Biosurfactants possess intriguing biological activity profiles, making them a promising candidate as anticancer agents. Moreover, they can serve as antineoplastic and antimicrobial agents against plant and human pathogens, making them an excellent therapeutic option for various infectious disorders.

Yeasts belonging to the genera *Candida*, *Metschnikowia*, *Starmerella*, and *Cryptococcus* are commonly found in solitary, stingless, bumble, and honey bees [14]. Among these genera, *Metschnikowia* and *Candida* (anamorphs) are the most prevalent taxa associated with bees and their flowers, as reported by Vega et al. [15]. Exploring yeasts associated with insect guts has the potential to reveal yeast diversity, their role in insect guts, and their possible applications in the pharmaceutical and industrial sectors.

This study aims to explore the yeast microbiota of the insect's gut and investigate their potential therapeutic applications such as antimicrobial and anticancer applications. The research specifically focuses on the physicochemical properties, characterization, antifungal, and anticancer activity of sophorolipids biosurfactants produced by two new isolates, CIG-11D^T and CIG-11X^T, which belong to the *Metschnikowia* clade and are designated as SL-11D and SL-11X, respectively. The study explores the sophorolipids molecules from these novel yeast strains, and the results show that they can be used as safe, stable, and biocompatible agents for both antimicrobial and anticancer purposes.

Materials and methods

Isolation of yeast strains

The gut-inhabiting yeasts were isolated from the bee using the previously described method [16]. Briefly, the insects were kept in a sterile 50 ml screw-capped tube for 2 days before the dissection. The insect samples were processed, purified, and preserved in 15% glycerol at − 80 °C and liquid nitrogen [17, 18].

Morphological and physiological characterization

Phenotypic characterization of strains CIG-11D^T and CIG-11X^T was performed using standard methods [19]. The carbon assimilation tests were performed using the Biolog YT microplate (Biolog, Inc., Hayward, CA) [17]. The carbon fermentation and nitrogen assimilation tests were performed using the standard method. The cell images were taken using a phase-contrast microscope (Olympus SC180 Tokyo, Japan). The sizes are given based on ten independent measurements.

Identification and phylogenetic analysis

DNA isolation, PCR amplification, and ITS and D1/D2 region sequencing were performed as described earlier [20]. The sequences corresponding to the type strains of closely related species were obtained from the GenBank database and subsequently aligned using CLUSTAL W (version 1.6) in the MEGA7 software [20]. Neighbor-joining trees were generated utilizing the D1/D2 region gene sequences, with the evolutionary distance calculated using the Kimura two-parameter correction model [21–23]. The confidence levels of the clades were determined through 1000 iterations of bootstrap analysis, with the resulting values expressed as percentages at nodes [24].

Physicochemical properties of SL-11D and SL-11X

Measurement of surface tension (ST) and critical micelle concentration (CMC)

The tensiometer was used to determine the ST of biosurfactant using the Wilhelmy plate method at 25 °C for 192 h, and deionized water was used to calibrate the equipment [25]. The CMC was calculated by measuring the biosurfactant's ST until it attained a constant value [20].

Stability studies

The stability of biosurfactants was observed in response to pH, salinity, and temperature. The stability of crude biosurfactants was investigated by subjecting them to varying temperatures (37°, 40°, 60°, 80°, 100°, and 121 °C for 15 min), pH levels (ranging from 2.0 to 12.0), and NaCl concentrations (ranging from 2 to 15% w/v) [3].

Sophorolipid production optimization using design of experiments (DOE)

The sophorolipids production from two strains, i.e., CIG-11D^T and CIG-11X^T, was optimized using the statistical designs Plackett–Burman (PB) and response surface methodology (RSM) constructed from Design-Expert® 11.0.0 (Stat-Ease Inc., Minneapolis, USA) software.

Plackett–Burman (PB)

It is a powerful, simple, and efficient fractional factorial experimental design for testing the most significant effects of different bioprocess variables and medium ingredients on the product yield [26, 27]. The current investigation focuses on optimizing sophorolipids production from two yeast strains of the same genus (i.e., CIG-11D^T and CIG-11X^T). As a result, identical factors were examined to optimize the bioprocessing of sophorolipids production in both strains. Therefore, in the PB experimental design, the ten different factors, i.e., yeast extract (A), peptone (B), malt extract (C), glucose (D), NaCl (E), temperature (F), incubation period (G), agitation rate (H), pH (I), and inoculum volume (J) were organized in different combinations and tested their low (−1) and high (+1) levels (Supplementary Table ST1). Using these factors, a design of 12 experiments was created, and the response, sophorolipids production, in terms of g/l, was calculated in each experiment ((Supplementary Table ST2 and Table 1). The effect of each variable was determined by plotting a Pareto chart using data obtained from the experimental design.

Response surface methodology (RSM)

RSM is a statistical tool used to evaluate the most significant factors and their interaction for optimizing the bioprocess and achieving the maximum yield of the desired product [28, 29]. The current investigation explored RSM's central composite design (CCD) to optimize sophorolipids production from CIG-11D^T and CIG-11X^T. Using CCD, the interactive effect of 4 most influencing factors [i.e., yeast extract (A), glucose (B), NaCl (C), and pH (D)] were checked at five various levels ($-\alpha$, −1, 0, +1, and $+\alpha$) by creating a design of 21 experiments (Table 2). The central value of each variable was obtained from the PB experimental design.

Table 1 PB design with experimental results for sophorolipid production from CIG-11D^T and CIG-11X^T

Run	A	B	C	D	E	F	G	H	I	J	Actual Sophorolipid yield from CIG-11D (g/l)	Predicted Sophorolipid yield from CIG-11D (g/l)	Actual Sophorolipid yield from CIG-11X (g/l)	Predicted Sophorolipid yield from CIG-11X (g/l)
1	4.5	2.5	4.5	15	5	37	108	270	3.1	1	7.80	9.40	8.28	9.17
2	1.5	2.5	1.5	15	5	37	108	90	9.3	3	9.50	9.15	9.20	8.58
3	1.5	2.5	1.5	5	5	13	36	90	3.1	1	8.70	8.62	8.25	8.19
4	4.5	2.5	1.5	5	15	13	108	270	3.1	3	11.00	11.19	10.35	9.96
5	4.5	7.5	4.5	5	5	13	108	90	9.3	3	5.60	5.02	4.65	4.38
6	1.5	7.5	4.5	5	15	37	108	90	3.1	1	13.80	12.86	12.40	11.57
7	1.5	7.5	4.5	15	5	13	36	270	3.1	3	11.50	11.08	11.25	10.78
8	1.5	2.5	4.5	5	15	37	36	270	9.3	3	9.35	10.94	8.35	9.37
9	4.5	7.5	1.5	15	15	37	36	90	3.1	3	14.00	13.65	11.70	12.55
10	4.5	7.5	1.5	5	5	37	36	270	9.3	1	5.20	5.02	3.85	4.38
11	4.5	2.5	4.5	15	15	13	36	90	9.3	1	12.40	11.72	11.95	10.34
12	1.5	7.5	1.5	15	15	13	108	270	9.3	1	13.20	13.40	11.00	11.96

Table 2 A CCD matrix with actual and predicted values of the AMP production

Run	A	B	C	D	Actual Sophorolipid yield from CIG-11D (g/l)	Predicted Sophorolipid yield from CIG-11D (g/l)	Actual Sophorolipid yield from CIG-11X (g/l)	Predicted Sophorolipid yield from CIG-11X (g/l)
1	3	10	18.409	6.2	18.65	18.46	16.40	16.26
2	3	18.409	10	6.2	21.40	21.38	19.20	19.28
3	4.5	15	5	3.1	19.05	18.99	14.45	14.30
4	1.5	5	5	3.1	5.20	5.14	5.95	5.80
5	3	10	10	11.413	9.10	9.08	9.10	9.18
6	3	10	10	6.2	10.10	10.14	10.10	10.09
7	3	10	1.591	6.2	10.80	10.95	9.05	9.35
8	1.5	5	15	3.1	5.40	5.49	5.40	5.43
9	4.5	15	15	3.1	22.60	22.69	21.90	21.93
10	1.5	15	15	9.3	21.45	21.54	18.60	18.63
11	3	10	10	6.2	10.00	10.14	10.00	10.09
12	1.5	15	5	9.3	13.30	13.24	13.95	13.80
13	3	10	10	6.2	9.95	10.14	9.95	10.09
14	3	10	10	6.2	10.20	10.14	10.20	10.09
15	4.5	5	15	9.3	8.85	8.94	8.20	8.23
16	5.522	10	10	6.2	9.10	9.08	9.10	9.18
17	0.477	10	10	6.2	8.45	8.43	8.45	8.53
18	3	10	10	6.2	10.42	10.14	10.42	10.09
19	3	1.591	10	6.2	5.35	5.33	5.35	5.43
20	3	10	10	0.986	11.40	11.38	11.40	11.48
21	4.5	5	5	9.3	3.45	3.39	4.05	3.90

Validation of optimized conditions in a bioreactor

Sophorolipids production was assessed for two strains using optimized conditions in a 2 l bioreactor system with a working volume of 1 l (Dasgip, GmbH, Germany). The bioreactor system consisted of four parallel vessels, each with a capacity of 2 l, with one vessel allocated to each strain (CIG-11D^T and CIG-11X^T). The bioreactor was operated in batch mode, and polypropylene glycol (PPG) was employed as an antifoam agent to control foaming. Samples were collected every six h to measure cell density (OD_{600nm}) and sophorolipids production (g/l).

Purification and characterization of SL-11D and SL-11X

Production and purification

To extract the sophorolipids, the culture was grown for 72 h at 25 °C with agitation at 180 rpm, followed by centrifugation at 8000 rpm for 30 min. Extraction of the biosurfactant was performed by mixing cell-free supernatant with an equal volume of ethyl acetate (1:1 ratio) in a separating funnel. Subsequently, the organic layer was separated and dried under vacuum using a rotary evaporator at 45 °C [30]. This crude biosurfactant extract was purified with silica gel (60–120 mesh; Merck Dramstadt, Germany) manually packed in absolute methanol in the glass column with dimensions 45×3.5 cm^2. The column was loaded with 5 ml of crude biosurfactant (1 g) dissolved in methanol and eluted with methanol: chloroform (0–90% chloroform) gradient system at a 3.0 ml/min flow rate. Separately collected fractions were vacuum-dried using rota vapor (BUCHI Rota vapor R-200) at 45 °C, and the biosurfactant was dissolved in a minimal amount of methanol. After testing these fractions for antimicrobial activity, multiple runs pooled the active fractions, and the solvent was evaporated. Biosurfactants were re-suspended in methanol and used further for characterization studies.

Thin layer chromatography (TLC) analysis of biosurfactants

The biosurfactants SL-11D and SL-11X, along with a sophorolipids standard SL-S, were applied onto a silica gel plate (Merck DC, Silica gel 60) using a mobile phase consisting of chloroform: methanol: water (65:25:4, v/v). The silica plate was developed, with lipid detection achieved via iodine fumes and sugars detected using anthrone reagent [3]

Fourier transform infrared spectroscopy (FTIR)

Infrared spectroscopy assessed the functional groups of biosurfactants (FTIR system, Perkin Elmer, Branford, CT,

USA). FTIR analysis of the standard SL and the test biosurfactants SL-11D and SL-11X were conducted using ATR (Attenuated Total Reflectance) with a wavenumber precision of 0.01 cm^{-1} and a resolution of 4 cm^{-1}, with 32 scans performed in conjunction with atmospheric CO_2 [31]. For the background spectrum, all data have been rectified.

Liquid chromatography-mass spectrometry (LC–MS)

LC–MS (1260 Infinity HPLC, Agilent Technologies, USA) was performed with a reverse-phase column (250 mm × 10 mm, 150 Å, Waters), and SL-S standard, was used to identify biosurfactants SL-11D and SL-11X, and their structural homologs. Solvent A (water having 1% TFA) and solvent B (acetonitrile having 1% TFA) were used as a mobile phase. In HPLC, gradient elution was used, which consisted of 5–20% solvent B in 5 min, 20–80% B in 25 min, and reverse 80–50% B in 3 min. The mobile phase flow rate was kept constant at 3.0 ml/min. ESI–MS (Electrospray ionization- mass spectroscopy) was executed in positive ion mode, with a 200–700 m/z spectral range examined using Agilent Mass Hunter software [20].

Antimicrobial and hemolytic activity of SL-11D and SL-11X

Determination of minimum inhibitory concentration (MIC)

The microtiter plate dilution assay was used to determine the MICs of biosurfactants. Bacterial test strains used are *Staphylococcus aureus* (MTCC 1430), *Vibrio cholerae* (MTCC 3904), *Klebsiella pneumoniae* (MTCC 618), *Listeria monocytogenes* (MTCC 839), *Bacillus subtilis* (MTCC 121), *Pseudomonas aeruginosa* (MTCC 1934), *Bacillus cereus* (MTCC 9490), *Salmonella enterica* (MTCC 3232), *Micrococcus luteus* (MTCC 106), and *Escherichia coli* (MTCC 1610). Additionally, the antifungal activity of biosurfactants was tested against plant and human pathogens. viz. *F. solani* (MTCC 350), *Penicillium chrysogenum* (MTCC 160), *Colletotrichum gloeosporium* (MTCC 2190), *Alternaria brassicola* (MTCC 2102), *Myrothecium verrucaria* (MTCC 158), and *Botrytis cinerea* (MTCC 2349) using a technique of broth microdilution [32]. After 24 h (Bacteria) and 48 h (Fungi), the plate's absorbance was measured at 600 nm using a plate reader (BMG Labtech, Germany), and the MIC was recorded as the lowest concentration that inhibited 90% of growth. As a control, untreated wells (only blank medium) were compared with the treated wells (OD 600).

Hemolysis assay

A blood sample collected from a rabbit (New Zealand White) in a test tube containing EDTA was used for the hemolysis assay. The blood sample was centrifuged for 5 min at 1000*g* before being washed three times in phosphate buffer saline (PBS, pH 7.4) [33]. Erythrocyte suspension (10%) was prepared in 1X-PBS and incubated at 37 °C for 24 h with increasing biosurfactant concentrations. After centrifuging the samples, cell-free supernatants were used to examine erythrocyte lysis at a 405 nm wavelength. Negative and positive controls were PBS and 1% Triton X-100, respectively. Negative and positive controls were PBS and 1% Triton X-100, respectively.

Deciphering the mode of action of biosurfactants

Transmission electron microscopy (TEM)

The integrity of bacterial and fungal cell membranes was visualized through the TEM study. Briefly, 10^6 *K. pneumoniae* and *F. solani* cells were taken and washed using sterile PBS and treated with sophorolipids using 1X-MIC at 25 °C for 24 and 48 h, respectively. After treatment, cells were washed three times, dissolved in 50 µl of PBS, and pipetted onto the carbon-coated 300-mesh copper grid (Polysciences, United States). Images were captured using a JEM 2100 electron microscope, operated at 200 keV (JEOL) [34]. Magnification ranged from 10,000X to 30,000X.

PI uptake assay and Confocal laser scanning microscopy

Cells of *K. pneumoniae* and *F. solani* were grown in the liquid medium until the late logarithmic phase, and 10^6 cells were centrifuged for 5 min at 1000*g*, washed, and treated with biosurfactants for 24 and 48 h, respectively, at 25 °C. After treatment, cells were washed and stained with PI (10 μmol^{-1}) for 15 min, followed by three times washing with PBS [3]. At least 10,000 events were acquired and analyzed by flow cytometry. The experiment was performed three independent times. The same set of treated cells was imaged in a confocal laser scanning microscope (Nikon A1R) with a 60X oil immersion objective using 1 Airy unit aperture and compared with control untreated cells. Images were captured using a 60X magnification.

Evaluation of reactive oxygen species (ROS) and intracellular calcium ion ($Ca2^{+)}$ level

Cells of *K. pneumoniae* and *F. solani* from primary overnight grown culture were harvested with an OD_{600} of 0.1, washed with 1X-PBS, and treated with different concentrations of biosurfactant (0 to 200 µg/ml) along with control containing methanol and incubated for 24 and 48 h, respectively at 37 °C in shaking incubator at 180 rpm. After treatment, the cells were centrifuged and washed with 1X-PBS twice. ROS-specific dye H_2-DCFDA (2 µM) was added to the cells and further incubated for 30 min at 37 °C. The cells were washed twice with PBS,

and fluorescence was recorded in a spectrophotometer with 495 excitation and 535 emission.

The calcium level of *F. solani* was determined using Fluo-3-acetoxymethyl ester (Fluo-3-AM) dye. The treated cells were stained with 5 mM Fluo-3-AM dye for 30 min at 37 °C, washed twice with PBS, and evaluated by flow cytometry [35]. The experiment was performed three independent times.

Cell culture and maintenance

Human embryonic kidney cell line HEK 293T, the human epithelial cell line Caco-2, murine fibroblast cell line L929, and human lung adenocarcinoma epithelial cell line A549, were maintained on DMEM supplemented with 10% fetal bovine serum (Thermo Fisher Scientific, USA) in humidified 5% CO_2 at 37 °C. HEK 293 T (ATCC, CRL-316) and L929 were purchased from ATCC. The caco-2 cell line was a gift from Dr. Hemraj (CSIR-IMTECH), and the A549 cell line was gift from Dr. Shekhar Majumdar (CSIR-IMTECH).

Cell cytotoxicity assay

The cytotoxicity effect of SL-11D and SL-11X was assessed against the Caco-2, A549, HEK-293T, and L929 cell lines by MTT assay. The cells were grown for 24 h in a 96-well plate using 2×10^4 cells/well. Cells were treated with different concentrations of biosurfactants SL-11D and SL-11X for the next 24 h. 20 µl of MTT (3-(4,5-dimethylthiazol-2-yl)-2,5-diphenyltetrazolium bromide) reagent was added in each well, incubated for 4 h. Formazan crystals formed were dissolved in 40 µl DMSO/well, and growth of cells was quantified at 570 nm absorbance in a microplate reader. The percentage of cytotoxicity was calculated with respect to live cells [8].

In vitro migration assay

The L929 cell line was treated with SL-11D and SL-11X SLs and imaged using an inverted microscope at 0, 24, and 48 h. ImageJ software was used to quantify the percentage inhibition of wound closure by measuring the migrating area [36].

Immunofluorescence assay

A549 cells seeded in respective complete growth media on 8 well-chambered slides at a density of 3×10^4 cells/well. Cells were allowed to adhere for 12 h at 37 °C until a complete monolayer formed. Cells were treated with SLs for 24 h. Subsequently, cells were washed with PBS and fixed with 4% PFA (Paraformaldehyde) for 20 min, followed by blocking with 1% bovine serum albumin (BSA) at room temperature for 1 h. FITC conjugated phalloidin (1:100 v/v) was used to determine the distribution of F-actin. Cells were counterstained for 10 min with 4′,6-diamidino-2-phenylindole (DAPI) (1:1000 v/v) and were examined under a confocal microscope (Nikon A1R); Etoposide (10 nM) was used as a positive control [8].

Dual Staining acridine orange/ethidium bromide (AO/EB)

The AO/EB staining method of Kasibhatla et al. [37] was used to assess the morphological corroboration of necrosis/apoptosis in SLs-treated cells. In brief, cells at a density of 1×10^5 were grown in 12 well cell culture plate until they formed a complete monolayer, and then cells were treated with SLs for 24 h before being washed with PBS. Finally, ethidium bromide and acridine orange cocktail (100 µg/ml each dissolved in PBS) were used to stain the cells. After 5 min of incubation, treated cells were imaged under a confocal laser scanning microscope (Nikon A1R) with a 60X oil immersion objective and using 1 Airy unit aperture and compared with the control group.

Reactive oxygen species (ROS) measurement

To assess the effect of sophorolipids on ROS levels in the A549 cell line, approximately 5×10^4 cells were seeded in each well of 24 well plate and incubated at 37 °C, with 5% CO_2 for 24 h. Later, media was aspirated, and cells were washed with PBS three times, and plates were incubated at 37 °C for 3 h with varying concentrations of SL-11D and SL-11X in the fresh medium (DMSO 0.2% was used as vehicle control). After treatment, cells were washed with 1X-PBS. ROS-specific dye H_2-DCFDA (2 µM) was added to the cells and incubated for 30 min at 37 °C. The cells were washed twice with PBS, and fluorescence was recorded in a spectrophotometer with 495 excitation and 535 emission [8].

Apoptosis assay

Using annexin V-FITC and propidium iodide (PI), a double-staining apoptotic test, the morphological features of apoptotic/necrotic cell death were examined (Life Technology) [38]. 3×10^5 cells were seeded into 6 wells of tissue culture plate and kept to incubate overnight. After that, the culture plate is treated for 24 h with various concentrations of SLs. The cells were then trypsinized and centrifuged, and the pellets were rinsed in cold PBS. The cells were dissolved in an annexin binding buffer (500 µl) and treated for 5 min with annexin V-FITC 488 (5 µl). After incubation, cells were treated with 1 µl of PI (100 mg/ml) and incubated for another 5 min. FACS (Bekman coulter) was used to determine % of apoptotic cells after applying compensation controls.

Statistical and structural analysis

There were at least three replicates to calculate the average, and error bars were used to indicate standard deviations. ANOVA and Tukey tests were used to evaluate, with a 95% confidence level. MarvinSketch version 20.19 was used to draw the chemical structures of the biosurfactants for the current study (http://www.chemaxon.com/products/marvin/marvinsketch/).

Results and discussion

Delineation and identification of CIG-11D^T and CIG-11X^T

On pairwise sequence alignment of the sequence of the D1/D2 region, *Metschnikowia shirguli* differed from its closest match by 13.5% sequence divergence, and *Metschnikowia dubei* differed from its closest match by 3.1% sequence divergence. Two of the new species were placed in the *Metschnikowia* clade. The

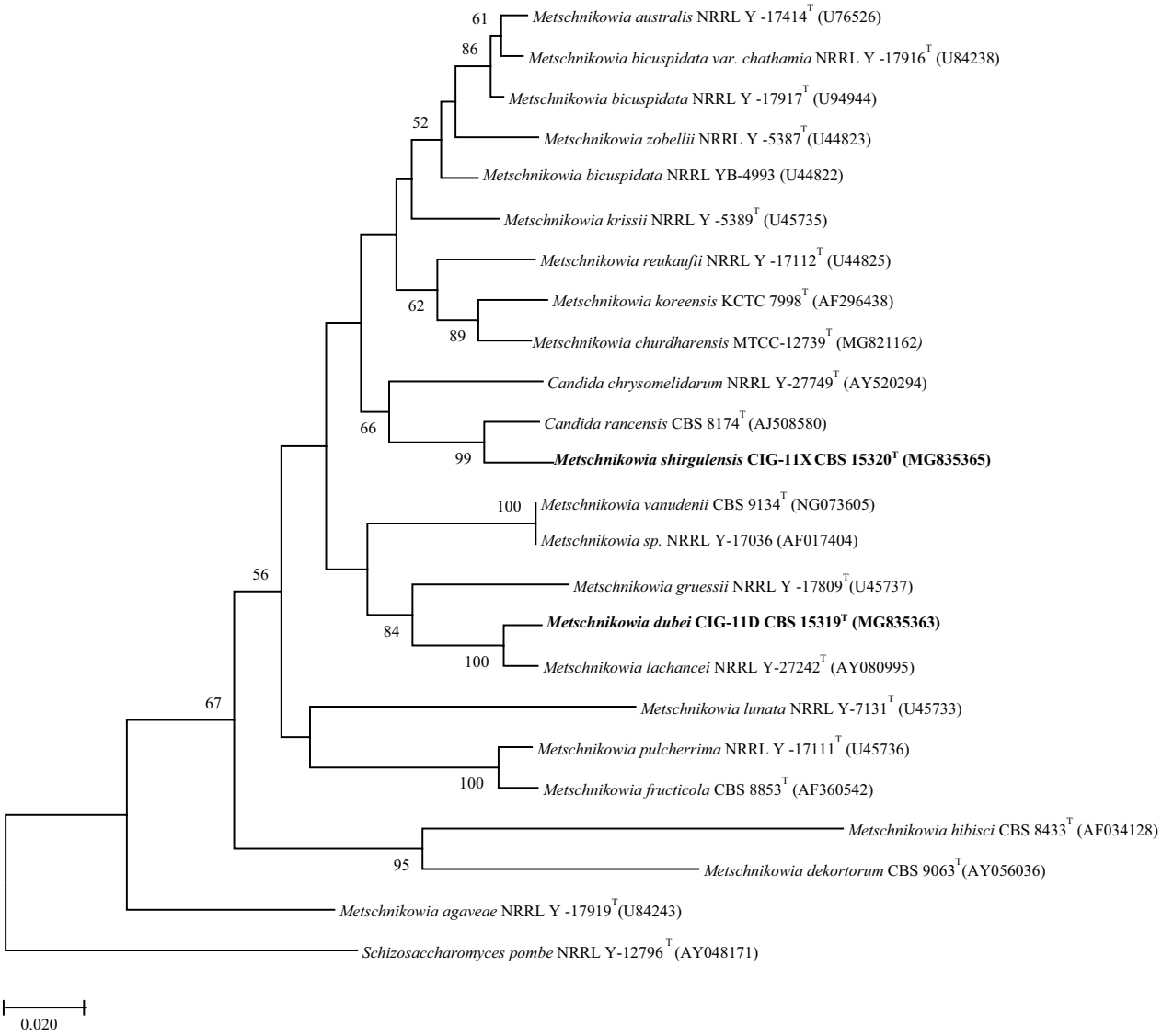

Fig. 1 Phylogenetic tree of the strains CIG-11D^T and CIG-11X^T. The phylogenetic tree was drawn using a neighbor-joining method based on the D1/D2 region of 26S rRNA gene sequences showing the relationship between *Metschnikowia shirgulensis* f. a. sp. nov., *Metschnikowia dubei* f. a. sp. nov. and related members of the genus *Metschnikowia*. *Schizosaccharomyces pombe* NRRL Y-12796^T (AY048171) was used as an out-group. Substitution per nucleotide position is bar 0.020. Bootstrap values (expressed as percentages of 1,000 replications) greater than 50% are given at nodes

Table 3 Physiological characteristics of strain *M. dubei* f.a., sp. nov., CIG-11D^T, *M. shirgulensis* f.a., sp. nov., CIG-11X^T and their closely related type strain

Physiological test	1	2	3	4	5	6
Fermentation of carbon compounds						
Glucose	+	+	+	+	+	+
Galactose	–	–	–	–	–	–
Maltose	+	–	–	–	+	–
Sucrose	+	–	w	–	+	–
Mannitol	+	–	–	–	+	NA
Assimilation of carbon compounds						
D-Galactose	–	+	–	+	–	–
D-Glucose	+	+	+	–	+	+
D-Glucosamine	–	+	–	w	–	–
D-Ribose	–	–	–	+	–	_
D-xylose	–	+	–	+	–	+
L-Arabinose	–	–	–	–	–	–
D-Arabinose	–	–	–	–	–	–
Maltose	+	+	–	–	w	+
D-Cellobiose	+	+	–	+	–	+
Melizitose	–	+	–	+	+	+
Arbutin	+	+	–	–	–	+
Salicin	–	+	–	+	–	+
Sucrose	+	+	–	+	–	+
Glycerol	–	+	–	+	–	+
Assimilation of nitrogen compounds						
Nitrite	w/d	–	w/d/+	–	w/d	–
Nitrate	w/d	–	–	–	–	–
Cadaverine	+	+	+	+	w/+	+
Creatine	w/d	w	w/d	–	–	–
Creatinine	w/d	w	w/d	–	d/+	–
D-Glucosamine	–	+	–	–	–	–
Ethlyamine	+	–	+	+	w/+	+
25 °C	+	+	+	+	+	+
30 °C	+	+	–	+	–	+
35 °C	–	+	–	–	–	–
37 °C	–	–	–	–	–	–
10% Na cl	–	+	–	–	w/+	+
16% NaCl	–	+	–	–	–	+
50% Glucose	+	++	+	–	+	+
60% Glucose	+/d/w	–	–	–	+	–
Acid production from glucose	–	–	–	–	–	–
Vitamin free	+	–	+	–	+	–

1, *M. dubei* f.a., sp. nov., CIG-11D^T; 2, *M. lachancei* (CBS 9131^T) (Gimenez-Jurado et al., 2003); 3, *M. shirgulensis* f.a., sp. nov., CIG-11X^T; and 4, *C. rancensis* (CBS 8174^T) (Mycobank Database)

+ positive, – negative, *w* weak, *d* delayed, *NA* not available, *v* Variable

neighbor-joining tree of novel yeast species from the *Metschnikowia* clade was constructed by using approximately 532 bp of D1/D2 region of 26S rRNA gene and taxa of all known near relatives of new species. On phylogenetic analysis, the *M. shirguli* formed a group with *C. rancensis* with 99% bootstrap values, and the *M. dubei* formed a group with *M. lachancea* with 100 bootstrap value (Fig. 1). Apart from the genetic variation, the related new species were different by assimilation tests of carbon and nitrogen compounds. Sucrose,

D-galactose, maltose, cellobiose, palatinose, D-gluconic acid, and D-galactose fermentation patterns were used to identify new yeast species.

M. dubei differed by 12 tests from its closest relative *M. Lachance,* and it failed to utilize D-glucosamine, D-ribose, and D-xylose, maltose, D-cellobiose, melezitose, and sucrose but was able to utilize nitrite, creatine, and creatinine as nitrogen sources. *M. shirguli* differed by 18 tests from *C. rancensis,* failing to utilize D-glucosamine, D-xylose, D-cellobiose, and arbutin (Table 3). These closely related species of *Metschnikowia* clade were previously isolated from flowers and associated insects [14].

In conclusion, the phylogenetic and biochemical test analysis made above indicated that the strain CIG-11D^T *Metschnikowia dubei* and CIG-11X^T *Metschnikowia shirgulensis* isolated from the gut of stingless bees represent two novel yeast species.

Strains MTCC 12740^T and MTCC 12741^T have been deposited in Microbial Type Culture Collection and Gene Bank (MTCC) Chandigarh, India, and Westerdijk Fungal Biodiversity Institute, Utrecht, The Netherlands, as strain; *Metschnikowia dubei* MTCC 12740^T = CBS 15319^T. The holotype is CBS 15319^T, and The Mycobank number of this species is MB 824670. The strain, *Metschnikowia shirgulensis* is deposited as MTCC 12741^T = CBS 15320^T. The holotype is CBS 15320 ^{T}. The Mycobank number of this species is MB 824671.

Physicochemical properties of biosurfactants

The biosurfactant's tensioactive properties primarily relate to its ability to reduce ST and CMC values. SL-11D and SL-11X biosurfactants effectively lowered the ST from 72.8 to 34 and 35.5 mN/m, respectively. Growth kinetics illustrate the biomass, yield, and ST of biosurfactants of strains CIG-11D^T and CIG-11X^T (Supplementary Fig. SF4A). The CMC values of SL-11D and SL-11X were 4 and 5 mg/ml, respectively, indicating that no further ST reduction was observed as the biosurfactant concentration was increased (Supplementary Fig. S4B). Table 4 shows the results of the emulsion stability after 24, 72, and 192 h.

The emulsion was stabilized and emulsified with crude, olive, and mineral oil using biosurfactants from CIG-11D^T and CIG-11X^T. E24 of CIG-11D^T and CIG-11X^T had the best emulsion stability against crude oil at 89% and 82%, respectively. Negative control (media) resulted in 0%, while positive control resulted in 100% of the E24 (Tween-20). ST was used to evaluate the stability of biosurfactants. In both cases, biosurfactant's ST reduction property was observed to be thermally stable up to 121 °C and 10% sodium chloride concentration. ST remained constant at pH 2.0, 4.0, 12.0, and 14.0, but at pH 6.0, 8.0, and 10.0, there was a decrease in ST in both SL-11D and SL-11X (Supplementary Fig. SF4C).

The promising biosurfactant is anticipated to reduce ST to nearly 35 mN/m. Consequently, strains CIG-11D^T and CIG-11X^T reduced ST below 36 mN/m, indicating potential biosurfactant production. *Pediococcus dextrinicus* produces a biosurfactant with a CMC value comparable to our study [5]. CMC is a fundamental feature of the surface-active compound. It is characterized as the minimal concentration of biosurfactant required to yield maximum reduction in ST [39]. Various biosurfactant production patterns were observed through fermentation based on the biosurfactant-producing microbes and surfactant nature [40]. The growth curve was studied in the case of CIG-11D^T and CIG-11X^T to demonstrate the correlation between surface activity, biomass, pH, and biosurfactant yield. After 24 h of incubation, the reduction of surface tension was noticed. The highest biosurfactant production was noted at 72 h (exponential phase), recommending a growth-associated sophorolipids production. However, in our study, biosurfactant yield was higher, suggesting that secondary carbon sources might not play a fundamental role in biosurfactant production and indicating that it helps to make the biosurfactant production process more inexpensive by excluding further costs of the secondary source. SL-11D and SL-11X biosurfactants contributed a high percentage of E24 with crude oil and a low percentage of E24 with mineral oil. Similar findings were made with a biosurfactant derived from *Starmerella bombicola* [41]. Also, sophorolipids exhibited excellent stability across the temperature, pH,

Table 4 Emulsification index (EI) evaluated using biosurfactant produced from CIG-11D^T and CIG-11X^T grown at 25 °C, 180 rpm, 2% inoculum (v/v), 1% glucose (w/v), 1%NaCl (w/v) after 24h, 72h and 192 h

S.no	Hydrophobic substrates	Emulsification index 11D (%)			Emulsification index 11X (%)		
		24 h	72 h	192 h	24 h	72 h	192 h
1	Mineral oil	74 ± 0.11	74 ± 0.3	70 ± 0.12	71 ± 0.11	71 ± 0.3	68 ± 0.12
2	Olive oil	75 ± 0.32	75 ± 0.2	73 ± 0.13	70 ± 0.32	70 ± 0.2	68 ± 0.13
3	Crude oil	89 ± 0.21	89 ± 0.32	84 ± 0.22	82 ± 0.21	82 ± 0.32	79 ± 0.22

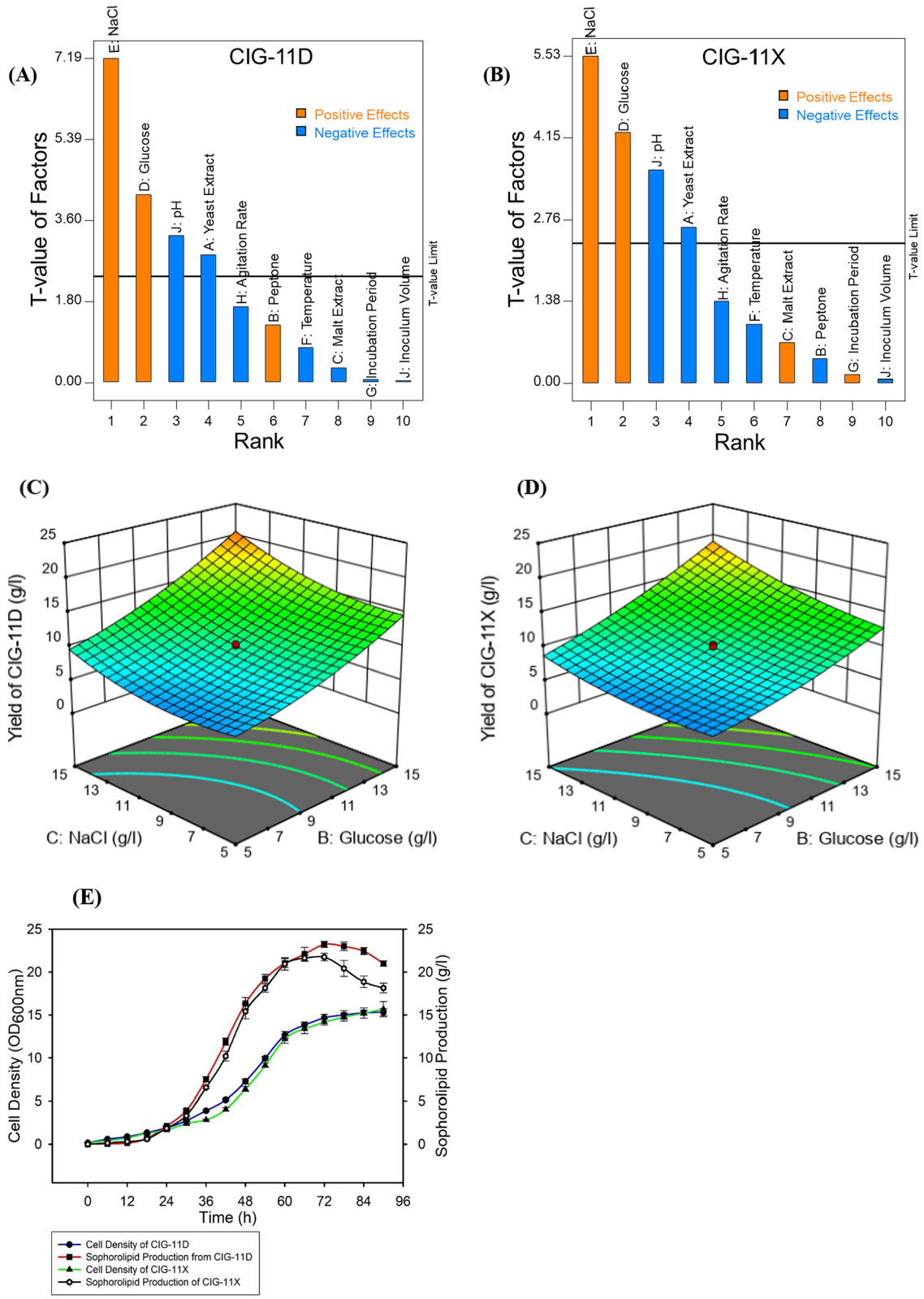

Fig. 2 Pareto chart depicting the effect of factors on sophorolipids production from CIG-11D^T (**A**), CIG-11X^T (**B**), response surface curves showing interactions between NaCl and glucose for sophorolipids production from CIG-11D^T (**C**), CIG 11X^T (**D**), and bioreactor profile of cell density and sophorolipids production from CIG-11D^T and CIG-11X^T (**E**)

and NaCl ranges tested, implying that it could be used in food formulations, microbial-enhanced oil recovery [42], and bioremediation [43]. Sarubbo et al. [44] achieved similar results using surfactants produced by *C. lipolytica* that exhibited ST reduction stability at variable temperatures, pH, and NaCl concentrations.

Sophorolipids production optimization

PB-based screening of most influencing factors for sophorolipids production

The optimization proceeds with PB experimental design to screen the effect of 10 factors (A to J) on sophorolipids production. In all these 12 runs, the sophorolipids production from CIG-11D^T and CIG-11X^T showed variations ranging from 5.20 to 14 g/l and 3.85 to 12.40 g/l, respectively, corresponding to the model's predicted value (Table 2 and Supplementary Fig. SF3A). The Pareto chart analysis revealed that 2 factors, NaCl and glucose, positively influenced sophorolipids production, while 2 factors, pH and yeast extract, had adverse effects (Fig. 2A and B).

Consequently, based on the Pareto chart, we identified 4 critical factors out of the 10 examined, including NaCl, glucose, pH, and yeast extract. These factors were found to have the most significant impact on sophorolipids production from the CIG-11D^T and CIG-11X^T strains. As a result, these 4 factors were selected for further investigation using CCD.

CCD-RSM for evaluating the interactive effects of the most significant factors

The 4 factors, i.e., yeast extract (A), glucose (B), NaCl (C), and pH (D), were set at 5 different levels and created a design of 21 experiments. The maximum productions of 22.60 and 21.90 g/l from CIG-11D^T and CIG-11X^T, respectively, were achieved in run 9, where yeast extract at 4.5 g/l, glucose at 15 g/l, NaCl at 15 g/l, and pH of 3.1 were provided in the production medium. The actual sophorolipids production in each experiment corresponded to the model's predicted values, which depicted its accuracy. The final sophorolipids productions of 22.6 g/l from CIG-11D^T and 21.90 g/l from CIG-11X^T which were 2.26-fold and 2.43-fold higher than initial sophorolipids production from CIG-11D^T and CIG-11X^T, respectively. The summary of optimized conditions is presented in Supplementary Table ST4.

The ANOVA of the CCD matrix for sophorolipids production from both strains was explored and presented in Supplementary Table ST3. The higher model F-values of 1144.13 (for CIG-11D^T) and 497.15 (for CIG-11X^T) and R^2 values of 0.99 (for both CIG-11D^T and CIG-11X^T) speculated that the current model is significant for producing sophorolipids from both strains [45]. A non-significant lack of fit (i.e., 1.49 for CIG-11D^T and 3.70 for CIG-11X^T) and adequate precision of 113.48 (for CIG-11D^T) and 83.03 (for CIG-11X^T) showed that the current model has a fair signal and can be used for sophorolipids production. The multiple regressions of the current model data points resulted in a second-order polynomial equation for the sophorolipids production from CIG-11D^T and CIG-11X^T.

The 3D response surface curve showing the interactive effect among NaCl and glucose showed that increasing the concentration of both factors increased sophorolipids production from CIG-11D^T and CIG-11X^T (Fig. 2C and D).

The interactive impact among other factors where NaCl and glucose were at central values (i.e., 10 g/l) yielded lower sophorolipids production (lower than 22.60 g/l from CIG-11D^T and 21.90 g/l from CIG-11X^T) (Data not shown). These findings suggest that increasing the model parameters may lead to higher sophorolipids production. However, the current model still yields substantial amounts of sophorolipids and can be considered an effective model for production purposes.

Evaluation of optimized conditions for sophorolipids production in a bioreactor

After optimizing the sophorolipids production at the shake flask level, we proceeded to scale up and validate the process at the bioreactor level. The bioreactor vessels were operated under optimized conditions, and we examined cell density and sophorolipids production every 6 h for a duration of 90 h. Our data revealed that the maximum sophorolipids production achieved was 23.24 g/l and 21.75 g/l after 72 h of batch fermentation for CIG-11D^T and CIG-11X^T, respectively (Fig. 2E).

These results indicate that the sophorolipids production from both strains in the bioreactor corresponds to that achieved in the shake flask, demonstrating their potential for large-scale production. Daverey et al. obtained a similar yield of sophorolipids of 23.29 g/l in a batch shake flask and 33.32 g/l in a bioreactor in *Starmerella bombicola* [46]. They obtained more yield in bioreactors because of the use of sunflower oil or olive oil [46]. During our study, a significant yield of sophorolipids was obtained in the bioreactor without using the secondary source (oil). This may make our production process more economical by avoiding the additional cost of the secondary source and further downstream process of sophorolipids. Moreover, further investigations employing fed-batch and continuous mode studies could potentially enhance sophorolipids production.

Characterization of biosurfactant SL-11D and SL-11X

Thin-layer chromatography (TLC)

TLC was used as a preliminary methodology for the compositional analysis of biosurfactants. The TLC chromatogram revealed a biosurfactant chemical form compared to the conventional SL-S sophorolipids. Two spots with Rf values of 0.657 and 0.710 were detected in SL-S. Sen et al. [3] obtained similar Rf values for acidic and lactonic forms in SL produced by *R. babjevae*, separated using the same mobile phase as in this study (Supplementary Fig. SF2).

FTIR

FTIR spectra of SL-S, SL-11D, and SL-11X were analyzed to check the functional groups (Supplementary Fig. SF5). The absorption of SL-11D biosurfactant at 2970.6 cm^{-1} and 2931.97 cm^{-1} and SL-11X biosurfactant at 2932.09 cm^{-1} and 2970.77 cm^{-1} respectively, be similar to asymmetrical stretching (ν_{as} CH_2) and symmetrical stretching (ν_s CH_2) of the methylene group. C=O lactone group of SL-11D and SL-11X represents the absorption at 1675.70 cm^{-1} and 1675.62 cm^{-1}, respectively. Strong absorption at 3339.72 cm^{-1} and 3337.20 cm^{-1} of SL-11D and SL-11X represented the O–H stretch. C(=O)–O–C= stretch in lactone was determined by absorption at 1160.53 cm^{-1} (SL-11D) and 1160.61 cm^{-1} (SL-11X). Carboxylic acid stretch in-plane bending is reflected in the absorption at 1467.09 cm^{-1} and 3339.72 cm^{-1}, which could be typical of acidic sophorolipids in SL-11D, whereas at 1466.95 cm^{-1} and 3337.20 cm^{-1} represents typical acidic sophorolipids in SL-11X. At 1675 cm^{-1} and 950 cm^{-1} (C=O and C–O–H, respectively), the biosurfactants SL-11D and SL-11X differed from the standard. FTIR data reveals that the biosurfactant from SL-11D and SL-11X is a combination of acidic and lactonic SLs. The presence of acidic SL was confirmed by the presence of two bands at 3339.79 and 1466.8 cm^{-1}, which are frequently associated with acidic SL in the literature [47].

LC–MS

Samples from the SL-11D, SL-11X, and the SL-S standard were analyzed using LC–ESI–MS in positive mode. The sodiated and protonated adduct ions were found in the samples and the standard. Biosurfactants SL-11D and SL-11X, MS were analyzed at various retention time points (Supplementary Fig. SF6A). At 7.32 min (SL-11D) and 7.23 min (SL-11X) retention time, a diacetylated sodiated form of acidic sophorolipids was analyzed. The $[M+H]^+$ ion of diacetylated acidic sophorolipids Ac_2AS $C_{16:0}+H^+$ and $[M+Na]^+$ ion of Ac_2AS $C_{16:0}+Na^+$ are the two peaks at *m/z* 678 and 700, respectively, were observed in SL-11D and SL-11X. In SL-11D, lactonic sophorolipids adducts with varied chain lengths of unsaturated fatty acids at retention time 12.7 min corresponds to *m/z* 448.27, 492.29, 531.36, 575.39, 619.41 and 663.44 resembles to Ac_2 sophorose $+Na^+$, LS $C_{10:1}$, LS $C_{11:1}+Na^+$, Ac_2 LS $C_{13:2}$, LS $C_{16:0}+Na^+$, and Ac_2 LS $C_{15:4}+Na^+$, respectively. In addition, lactonic sophorolipids at retention time 7.6 min corresponds to *m/z* 516 and 538, which resembles LS $C_{12:3}$ and LS $C_{12:3}+Na^+$ were observed in SL-11D. In SL-11X, the $[M+H]^+$ ion of diacetylated acidic sophorolipids Ac_2AS $C_{16:0}+H^+$ and $[M+Na]^+$ ion of Ac_2AS $C_{16:0}+Na^+$ are the two peaks at *m/z* 678 and 700 were observed. In SL-11X, lactonic sophorolipids adduct with varied chain lengths of unsaturated fatty acids at retention time 12.5 min corresponds to *m/z* 448.26, 487.34, 531.36, 575.39, 619.41, 663.44 and 707.46 resembles to Ac_2 sophorose $+Na^+$, LS $C_{10:3}$, LS $C_{11:1}+Na^+$, Ac_2 LS $C_{13:2}$, LS $C_{16:0}+Na^+$, Ac_2 LS $C_{15:4}+Na^+$, and Ac_2 LS $C_{18:3}+Na^+$ respectively. Ac_2 sophorolactone with a C_{18} saturated fatty acid moiety has peaks at m/z 710.4 and 688 with RT 13.1 min corresponding to [M+Na]+ and [M+H]+ ions observed in SL-S standard. Lactonic and acidic SLs with various side chains of fatty acids were found to have protonated and sodiated ions in our study (C10-C18). LC–MS study revealed similar sophorolipids ions with a heterogeneous composition in *R. babjevae* YS3 [3]. Table 5 shows the finalized list of sophorolipids homologs found in SL-11D and SL-11X, whereas their

Table 5 Type of sophorolipid homologues, Molecular mass and chemical structure of sophorolipid produced by the SL-11D and SL-11X, along with sophorolipid standard, 1,4′′-sophorolactone 6′,6′′-diacetate (SL-S) as determined by LC–MS

Homologue	Formula	Molecular mass	Type of SL	Source
SL-11D				
LS-$C_{10:1}$	$C_{22}H_{36}O_{12}$	492.52	Lactonic	SL-ClG-11D
LS-$C_{11:0}$	$C_{23}H_{40}O_{12}$	508.25	Lactonic	SL-ClG-11D
AcLS-$C_{13:3}$	$C_{25}H_{42}O_{12}$	534.26	Lactonic	SL-ClG-11D
LS-$C_{18:5}$	$C_{30}H_{44}0_{12}$	596.8	Lactonic	SL-ClG-11D
Ac_2AS-$C_{16:0}$	$C_{32}H_{56}O_{15}$	678.8	Acidic	SL-ClG-11D
Ac_2 LS-$C_{15:3}$	$C_{27}H_{41}O_{12}$	572.5	Lactonic	SL-ClG-11D
SL-11X				
LS-$C_{10:3}$	$C_{22}H_{32}O_{12}$	488.18	Lactonic	SL-ClG-11X
LS-$C_{11:0}$	$C_{23}H_{40}O_{12}$	508.25	Lactonic	SL-ClG-11X
AcLS-$C_{13:3}$	$C_{25}H_{42}O_{12}$	534.26	Lactonic	SL-ClG-11X
LS-$C_{18:5}$	$C_{30}H_{44}0_{12}$	596.8	Lactonic	SL-ClG-11X
Ac_2 LS-$C_{15:3}$	$C_{27}H_{41}O_{12}$	572.5	Lactonic	SL-ClG-11X
Ac_2 LS-$C_{18:3}$	$C_{34}H_{54}O_{14}$	686.3	Lactonic	SL-ClG-11X
Ac_2AS-$C_{16:0}$	$C_{32}H_{56}O_{15}$	678.8	Acidic	SL-ClG-11X
Ac_2LS-$C_{18:1}$	$C_{34}H_{56}O_{14}$	688.8	Lactonic	SL-S

LS lactonic sophorolipid, *AS* acidic sophorolipid, *Ac* acetyl group, *SL-11D* sophorolipid produced by *Metschnikowia dubei*, *SL-11X* sophorolipid produced by *Metschnikowia shirgulensis*, *SL-S* sophorolipid standard

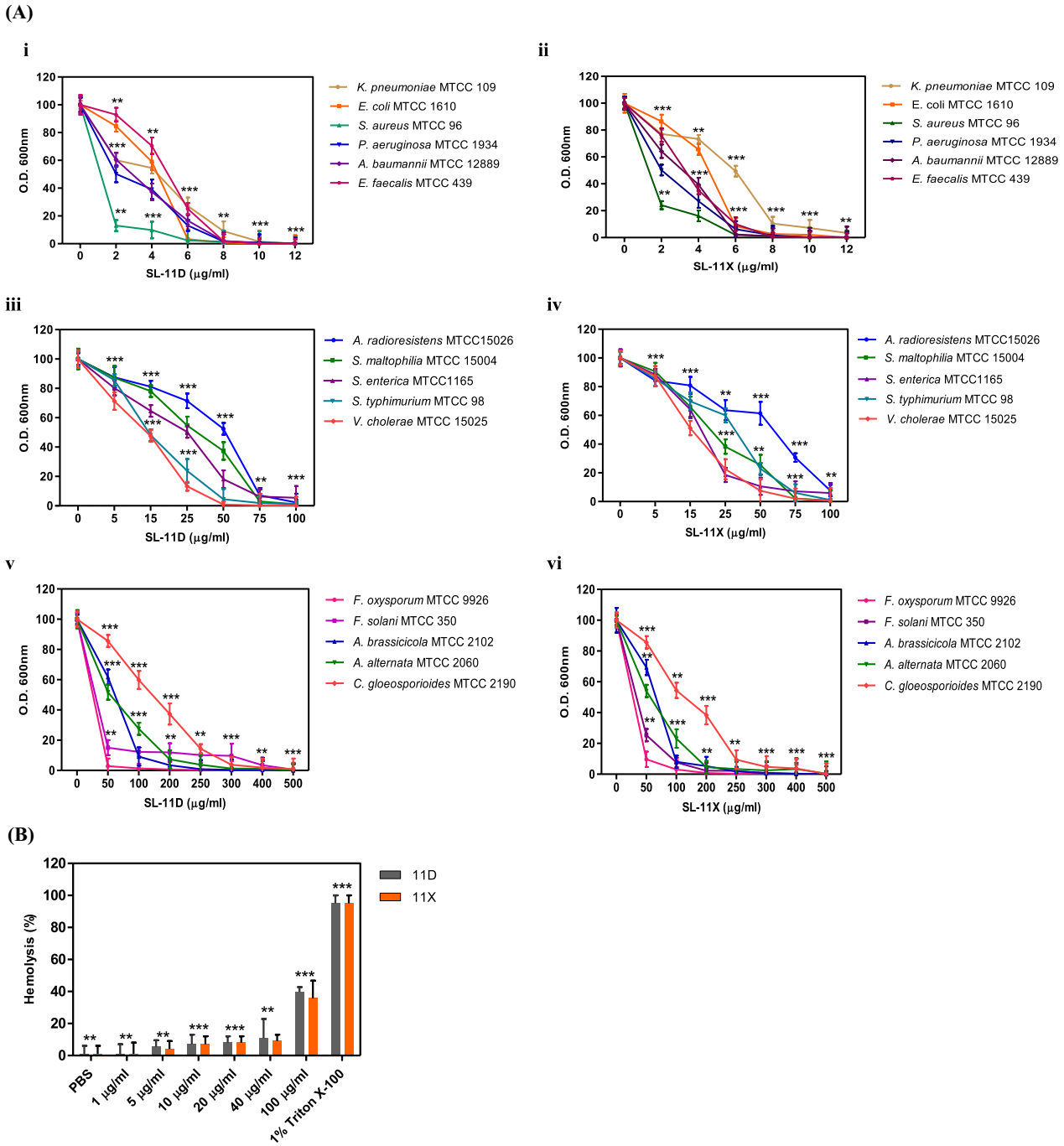

Fig. 3 Determination of minimum inhibitory concentrations (MICs) and hemolysis activity of SL-11D and SL-11X in a microtiter plate assay performed in triplicate. (**A**) MICs against test strains, clinical strains, and pathogenic fungal strains. (**B**) Hemolysis assay of biosurfactant using RBCs of a rabbit. Purified biosurfactants, RBC samples, and bacterial cells were prepared in PBS. All the experiments are executed in triplicate. Bars show standard deviation. P values are shown above each bar (significance was at a P level of 0.05)

corresponding lowest energy structures are mentioned in Supplementary Fig. SF6B.

Antimicrobial and hemolytic activity of SL-11D and SL-11X

With respect to Gram-negative and Gram-positive bacteria, the biosurfactants SL-11D and SL-11X had a

wide-ranging effect. The MIC analysis of SL-11D and SL-11X (Fig. 3A) revealed that they are more effective against *S. aureus* at concentrations of 2 (Fig. 3A i) and 5 µg/ml (Fig. 3A ii), respectively, and against *K. pneumoniae* at concentrations of 7 (Fig. 3A i) and 8 µg/ml (Fig. 3A ii), respectively. Figure 3A iii and iv illustrated that SL-11D and SL-11X were active against clinical isolates at a 50–100 µg/ml concentration. SL-11D and SL-11X biosurfactants exhibit activity against plant and human fungal pathogens, analyzed on MIC basis (50–500 µg/ml). Biosurfactants demonstrated promising antifungal activity against *F. solani* and *F. oxysporum*, as evidenced by their low MIC values (Fig. 3A v and vi).

Antimicrobial activity of sophorolipids against Gram-positive bacteria, including *Staphylococcus epidermidis*, *Bacillus subtilis*, *Streptococcus faecium*, *Staphylococcus aureus*, *Corynebacterium xerosis*, and *Propionibacterium acnes* has been previously reported [48]. Antimicrobial activity was observed for SL-11D and SL-11X against both Gram-negative and Gram-positive species in this study. Sophorolipids are bactericidal through multiple mechanisms, including the modification and destabilization of cellular membrane permeability. This suggests that SL-11D and SL-11X may be useful as antibacterial agents against bacterial pathogens. Dengle-Pulate et al. [49] reported that 1 and 6 µg/ml concentrations completely inhibited *B. subtilis* and *S. aureus*, respectively, and comparable results were observed in our study. Sen et al. [3] reported that 125 µg/ml of sophorolipidinhibited *F. oxysporum*. Hipolito et al. [50] reported that 729 µg/ml sophorolipids inhibited *F. oxysporum*. The literature lacks sophorolipid's effect on food spoilage and pathogenic fungi. Consequently, these findings may help establish how to implement sophorolipids as a natural and alternative fungicide agent in the food industry to control food-borne fungi and their toxic substances. Figure 3B shows, however, at high MIC values, no RBCs (Red blood cells) were lysed in the hemolysis assay, and similar results were observed by Hipolito et al. [50].

Mechanism of action of SL-11D and SL-11X against *K. pneumoniae*

Transmission electron microscopy

To understand the killing ability of SL-11D and SL-11X, treated and untreated *K. pneumoniae* cells were observed under TEM. Untreated *K. pneumoniae* MTCC 618 cells exhibited a smooth surface and were intact and healthy. There were cell wall irregularities in cells treated with SL-11D and SL-11X, such as cell lysis and wall rupture (Fig. 4A i).

Membrane permeability assay

The permeability of the cell membrane as a result of SL-11D and SL-11X treatment was observed by PI staining, followed by flow cytometry (Fig. 4A ii) and visualization under CLSM (Fig. 4A iii).

Compared to the 0.92% PI-positive untreated cells, flow cytometric analysis showed that the SL-11D and SL-11X (1X-MIC) treatments resulted in 99.01% and 98.06% permeabilized cells, respectively. The CLSM imaging revealed increased red fluorescence in treated *K. pneumoniae* cells due to the permeation of PI, implying cell death. Untreated cells, on the other hand, showed no fluorescence, indicating that they were healthy.

Production of reactive oxygen species in the presence of SL-11D and SL-11X

The level of ROS quantified in SL-11D and SL-11X treated *K. pneumoniae* cells were significantly higher than the non-treated cells, as shown in Fig. 4A iv, indicating a higher level of ROS generated in *K. pneumoniae* cells upon exposure to SL-11D and SL-11X.

However, when cells were treated with *N*-acetylglucosamine (NAG; ROS-quencher), the fluorescence of H_2-DCFDA was quenched. These findings strongly suggested that treatment with sophorolipids resulted in significant ROS generation, possibly resulting in bacterial cell death.

Several glycolipids possess antimicrobial, anticancer, and antiadhesive properties, including rhamnolipid,

(See figure on next page.)

Fig. 4 Increased permeabilization of cell membrane of *K. pneumoniae* MTCC 618 cells after SL-11D and SL-11X treatment (**A**). (**i**) Transmission electron microscopy images of untreated and treated *K. pneumoniae* cells. (**ii**) Flow cytometry evaluation of the bacterial membrane integrity using PI. (**iii**) Fluorescence microscopy of *K. pneumoniae* stained with PI after treatment with SL-11D and SL-11X at 1X-1 × MIC. (**iv**) SL-11D and SL-11X induced ROS production in *K. pneumoniae*. Alteration of *F. solani* MTCC 350 membrane integrity due to SL-11D and SL-11X treatment. All the experiments are executed in triplicate. Bars show standard deviation. P values are shown above each bar (significance was at a P level of 0.05). (**B**). (**i**) Effect of SL-11D and SL-11X on *F. solani* mycelium visualized by TEM. (**ii**) Evaluation of PI-positive population by flow cytometry after treatment with SL-11D and SL-11X. (**iii**) CLSM of *F. solani* cells treated with 5X-MIC of SL-11D and SL-11X and stained with PI. (**iv**) SL-11D and SL-11X stimulate the ROS production. (**v**) SL-11D and SL-11X elevate the intracellular calcium (Ca^{2+}) ions level

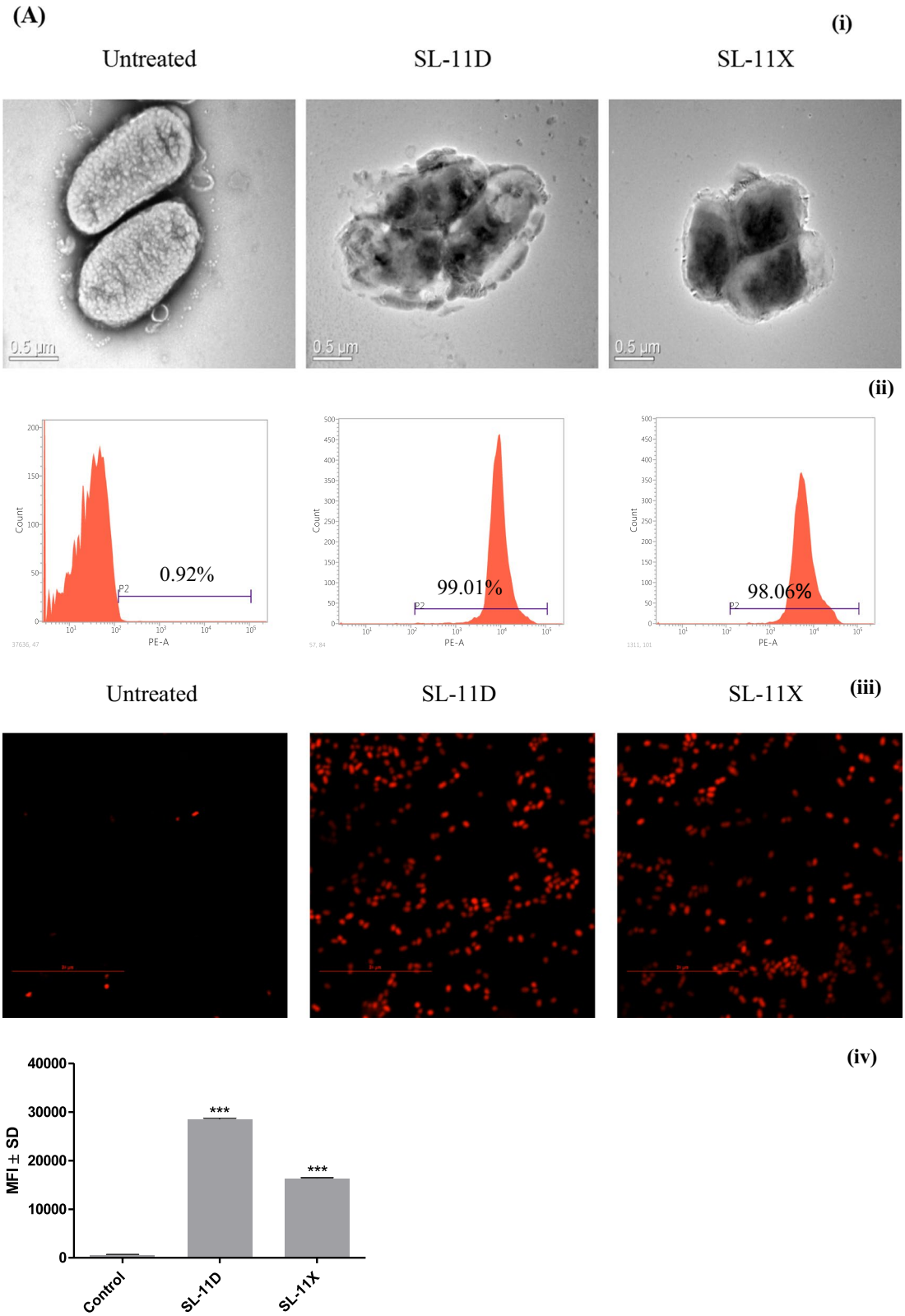

Fig. 4 (See legend on previous page.)

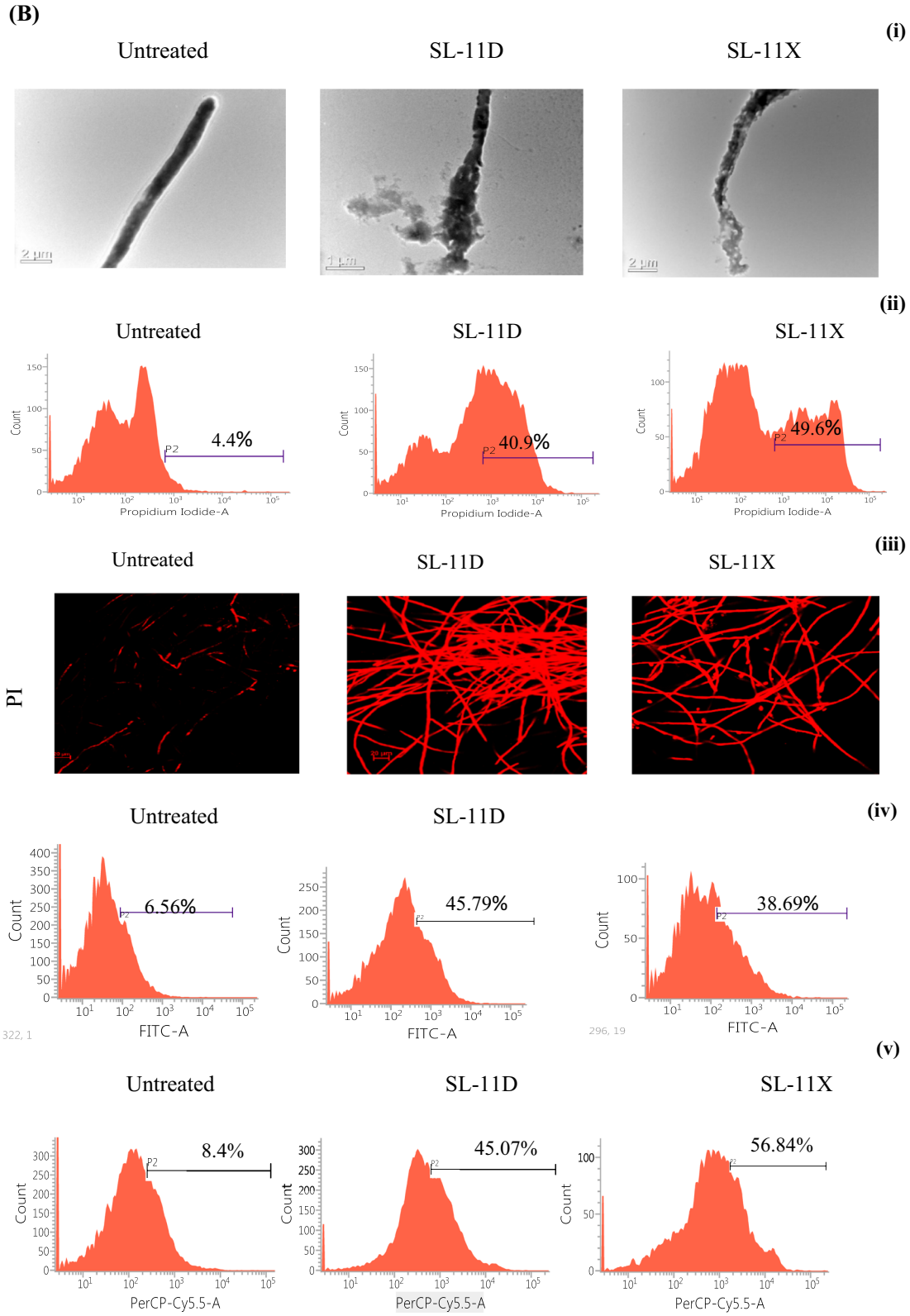

Fig. 4 continued

sophorolipids, mannosyl erythritol lipid, and other glycolipids [8]. So, we attempted to evaluate these properties using sophorolipids SL-11D and SL-11X and explored their possible mode of action. The mechanism of action of sophorolipids has been demonstrated for the first time against *K. pneumoniae* via., TEM, PI uptake assay, and ROS determination. As per the literature, the antimicrobial mode could be outlined as ROS production, efflux pump inhibition, and increased cell membrane permeability [51]. Normal cells produce ROS during metabolism and oxygen respiration; however, redox-cycling agents, antibiotics, and membrane disruptors increase ROS production [52]. Consequently, oxidative stress occurs when a cell cannot detoxify excessive ROS, resulting in cell death via necrosis or apoptosis. Sophorolipids from *C. bombicola* demonstrate antibacterial activity against gram-positive and gram-negative bacteria by disrupting cell membranes, altering cell morphology and structure, and increasing membrane permeability [53]. Sikha et al. noted that treatment of *Vibrio cholerae* with sophorolipid-capped nanoparticles induces the production of reactive oxygen species (ROS), leading to upregulation of ROS-responsive genes, alterations in membrane permeability, leakage of intracellular proteins, and ultimately, cell death [54]. The current study yielded comparable results.

Mechanism of action of SL-11D and SL-11X against F. solani

Transmission electron microscopy

TEM analysis was carried out to visualize the effect of SL-11D and SL-11X on the mycelia of *F. solani* MTCC 350. We found that SL-11D and SL-11X disturbed the integrity of the mycelia of *F. solani* (Fig. 4B i), causing pore formation compared to untreated mycelia of *F. solani*.

Membrane permeability assay

Cell membrane integrity is lost due to SL-11D and SL-11X treatment, and PI gets into the cells through the permeabilized cell membrane as measured by flow cytometry. Compared to 4.4% PI-positive untreated cells, the cells treated with 5X-MIC of SL-11D and SL-11X had 40.9% and 49.6% permeabilized cells, respectively (Fig. 4B ii). CLSM images (Fig. 4B iii) demonstrated that PI permeation increased red fluorescence following treatment with SL-11D and SL-11X at 5X-MIC, indicating cell death. Whereas untreated samples exhibited no red fluorescence, indicating the presence of healthy cells.

The mycelium, essential for fungal reproduction, is susceptible to changes in cell integrity, impacting the pathogenicity of the fungus. Sophorolipids have been shown to significantly modify fungal mycelia morphology, potentially disrupting the cell membrane's phospholipid layer owing to their amphiphilic properties [50]. Previously, Hipolito et al. demonstrated surface irregularities and deformed cell structure of fungal mycelia on treatment with sophorolipids produced by *S. bombicola* [50].

ROS and Ca^{2+} measurement in F. solani

According to the literature, SL causes cell death by activating various stress response pathways, which leads to cell lysis [35]. Cellular stress due to external stimuli results in the production of ROS in the cell. Increased ROS can further target endoplasmic reticulum (ER)-based calcium channels, increasing calcium release and ROS levels [55].

The ROS generation was increased upon treatment with SL-11D and SL-11X (Fig. 4B iv). ROS generation was increased 6.9-fold (45.79% of the total cell population) and 5.8-fold (38.69% of the total cell population) in the presence of 100 µg/ml SL-11D and SL-11X, respectively, when compared to control (6.56% of the cell population). Additionally, we observed that cells treated with 100 µg/ml SL-11D and SL-11X had 5.3-fold (45.07% of the total cell population) and 6.7-fold (56.84% of the total cell population, respectively, increased Ca^{2+} levels when compared to control cells (8.45% of the total cell population) (Fig. 4B v).

These findings strongly suggested that SLs produce a high level of ROS in cells, which may result in cell death via apoptosis or necrosis. Sophorolipids induce ER stress by increasing HAC1 (a marker of ER stress) transcript levels, leading to calcium efflux from the ER into the cytoplasm and activation of the high osmolarity glycerol (HOG) mitogen-activated protein kinase (MAPK) pathway. These stress responses culminate in necrosis and cell death [35]. Similar findings of increased ROS production and elevated Ca^{2+} levels were observed in *C. albicans* upon treatment with SLs from *S. bombicola* [35].

Mechanism of action of SL-11D and SL-11X against Cancerous cell line

Cytotoxicity and migration potential of SL-11D and SL-11X

To check the cytotoxic and migration potential for 24 h, cell lines Caco-2, HEK-293 T, L929, and A549 were treated with SL-11D and SL-11X at various concentrations (0–100 µg/ml), as shown in Fig. 5A. Neither SL-11D nor SL-11X exhibited any cytotoxicity on Caco-2, HEK-293T and L929 cell lines up to 100 µg/ml. Similarly, Ribeiro et al. also observed SLs' non-cytotoxicity on non-cancerous cells [56].

The cytotoxic effect of SL-11D and SL-11X on the A549 cancerous cell line was observed. Results revealed a

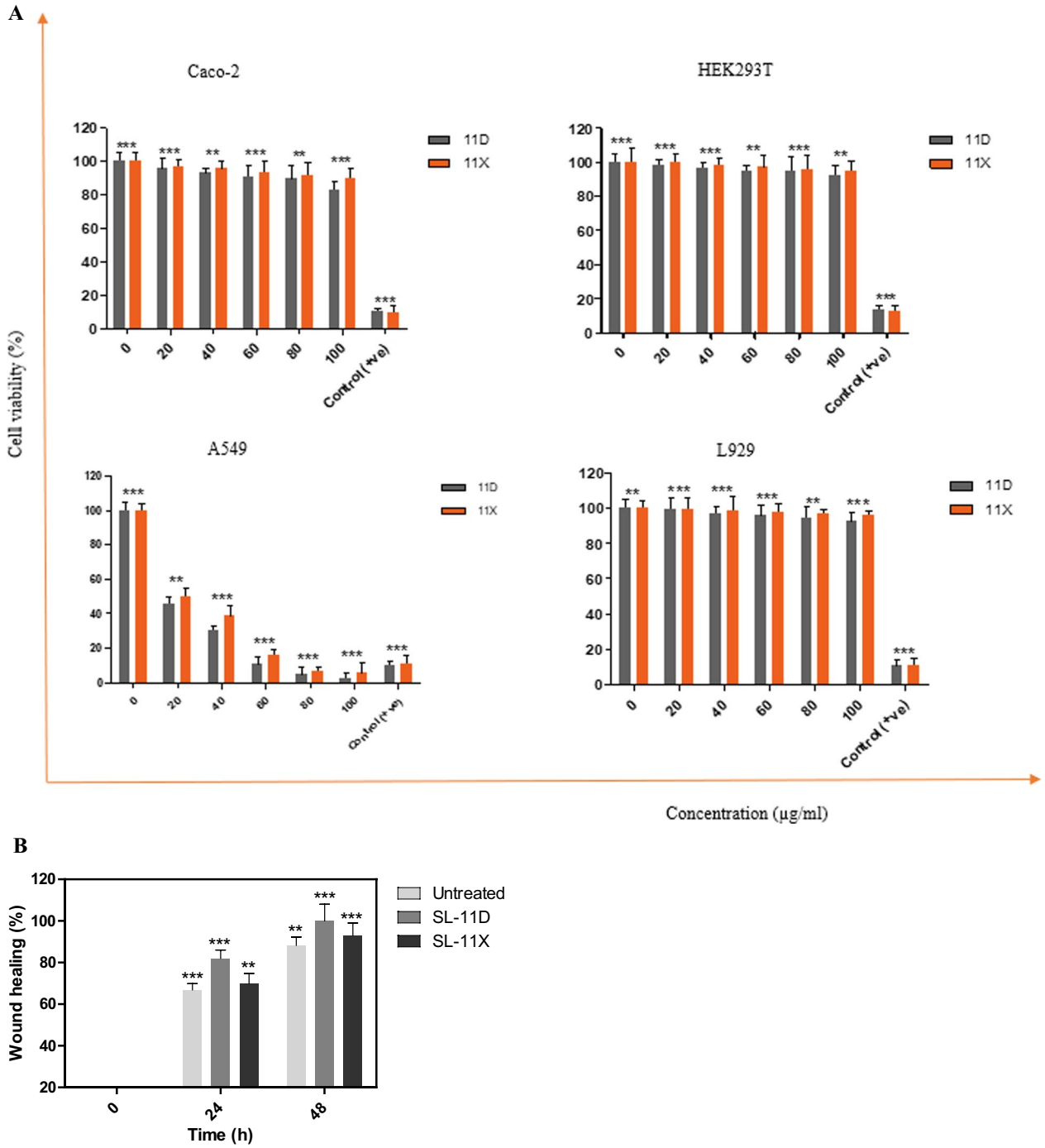

Fig. 5 The cytotoxic effect of SL-11D and SL-11X on (**A**) gut epithelial cell line Caco-2, human embryonic kidney 293 cells, fibroblast cell line L929, and A549 for 24 h treatment. The figure has been plotted with respect to DMSO vehicle control and done in triplicates, and the mean value has been shown. A p-value of < 0.05 was considered statistically significant, (**B**) the percentage of enclosed area after wounding of L929 cells. and (**C**) representative images from the wound healing assay at 0, 24, and 48 h

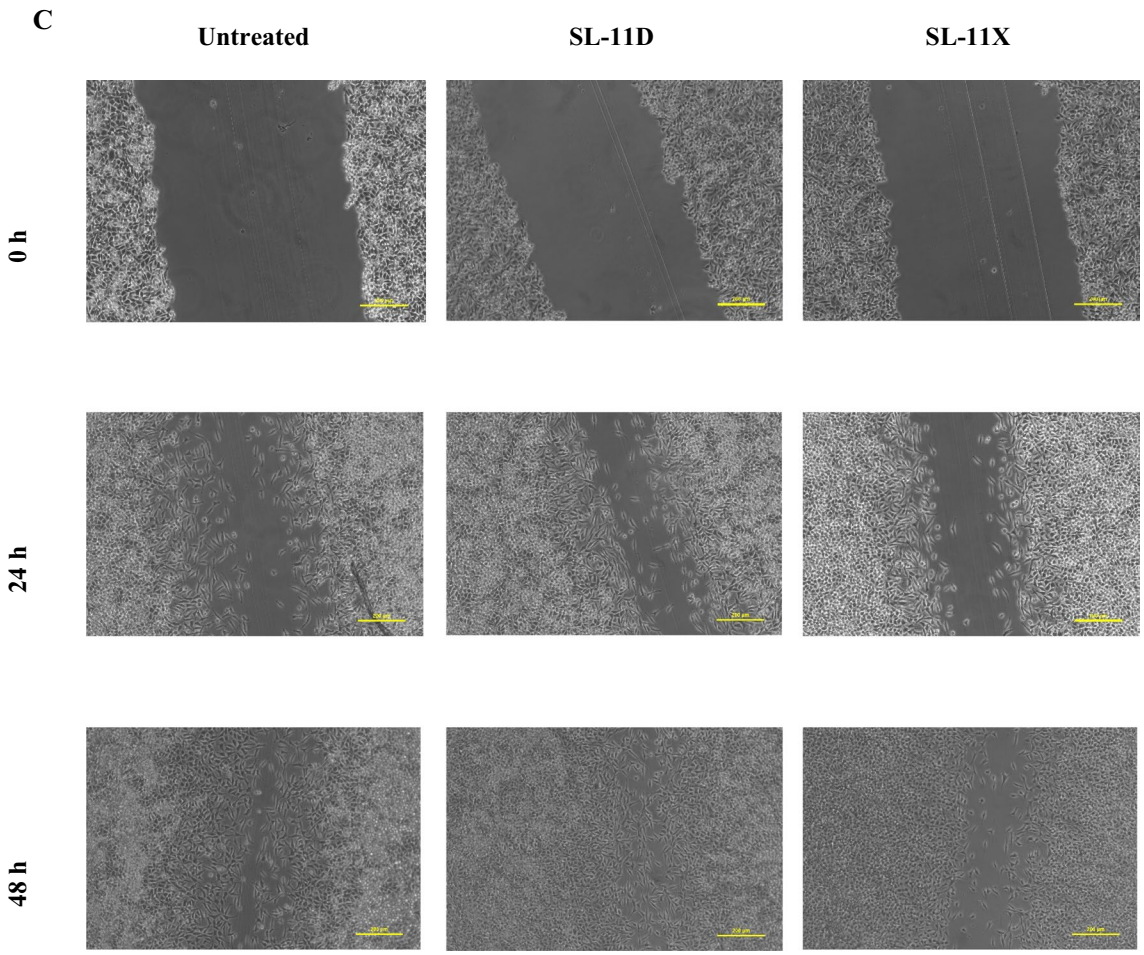

Fig. 5 continued

significant toxicity of sophorolipids at 50 µg/ml after 24 h of treatment.

A cell migration assay was conducted on the L929 cell line in vitro to assess the impact of sophorolipids on wound healing potential. The findings demonstrated a notable enhancement in human skin fibroblast migration upon the application of the optimal concentration (50 µg/ml) of SL-11D and SL-11X (Fig. 5B).

Sophorolipids were used to treat cultured cells, and then the cells were examined under a microscope to investigate the migration of cells (Fig. 5C). Maeng et al. [57] also found cell migration by SLs on a fibroblast cell line.

(See figure on next page.)

Fig. 6 The effect of sophorolipids biosurfactant on the actin cytoskeleton. (**A**) Cancer cells were treated with SL-11D and SL-11X and stained with anti-phyllodin antibodies to visualize the actin filament and 4′,6-diamidino- 2-phenylindole (DAPI) to visualize the nucleus, (**B**) Acridine orange (AO) and ethidium bromide (EB) staining of the cancerous cell after treatment of SL-11D and SL-11X. Red spots showed necrotic bodies, whereas dark green spots showed the appearance of the early stage of apoptosis. Etoposide was used as a positive control, (**C**) The estimation of ROS was measured by fluorimetric analysis, and the results were compared with DMSO control. Etoposide was used as a positive control, (**D**) Flow cytometry (FACS) analysis of Annexin V and PI-stained cancer cells after treatment with SL-11D and SL-11X to study the sophorolipids effect on apoptosis/necrosis. The lower left panel of each quadrant represents untreated control; the upper left panel shows the necrotic bodies, whereas the upper and lower right panel shows the late and early stages of apoptosis. Etoposide (25 nM) was used as a positive control, whereas DMSO was used as vehicle control. All the experiments were performed three times on three independent days, and (**E**) Percentage of apoptosis after treatment with SL-11D and SL-11X. All experiments were conducted in triplicate. Error bars represent standard deviation, with significance indicated above each bar ($P < 0.05$)

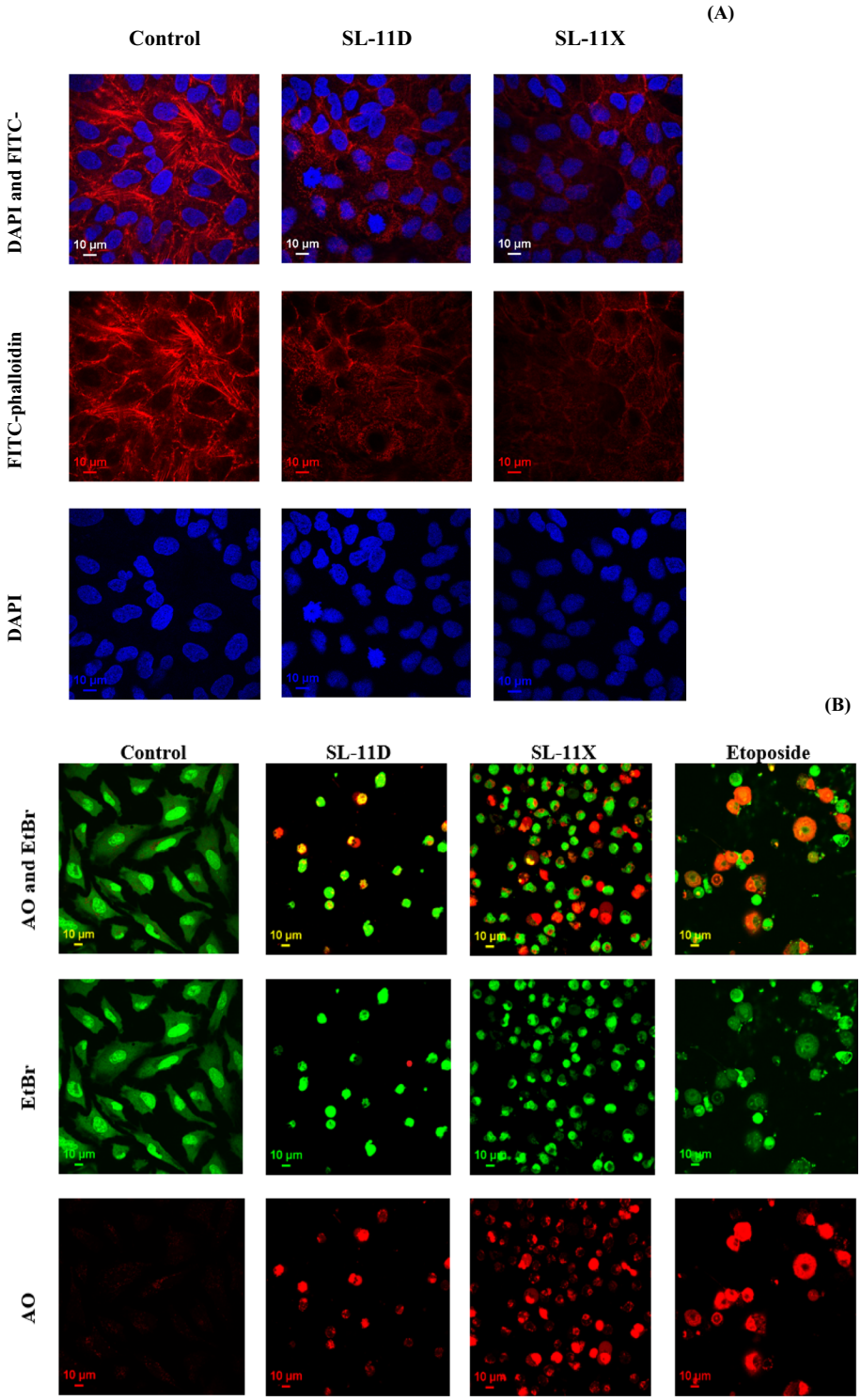

Fig. 6 (See legend on previous page.)

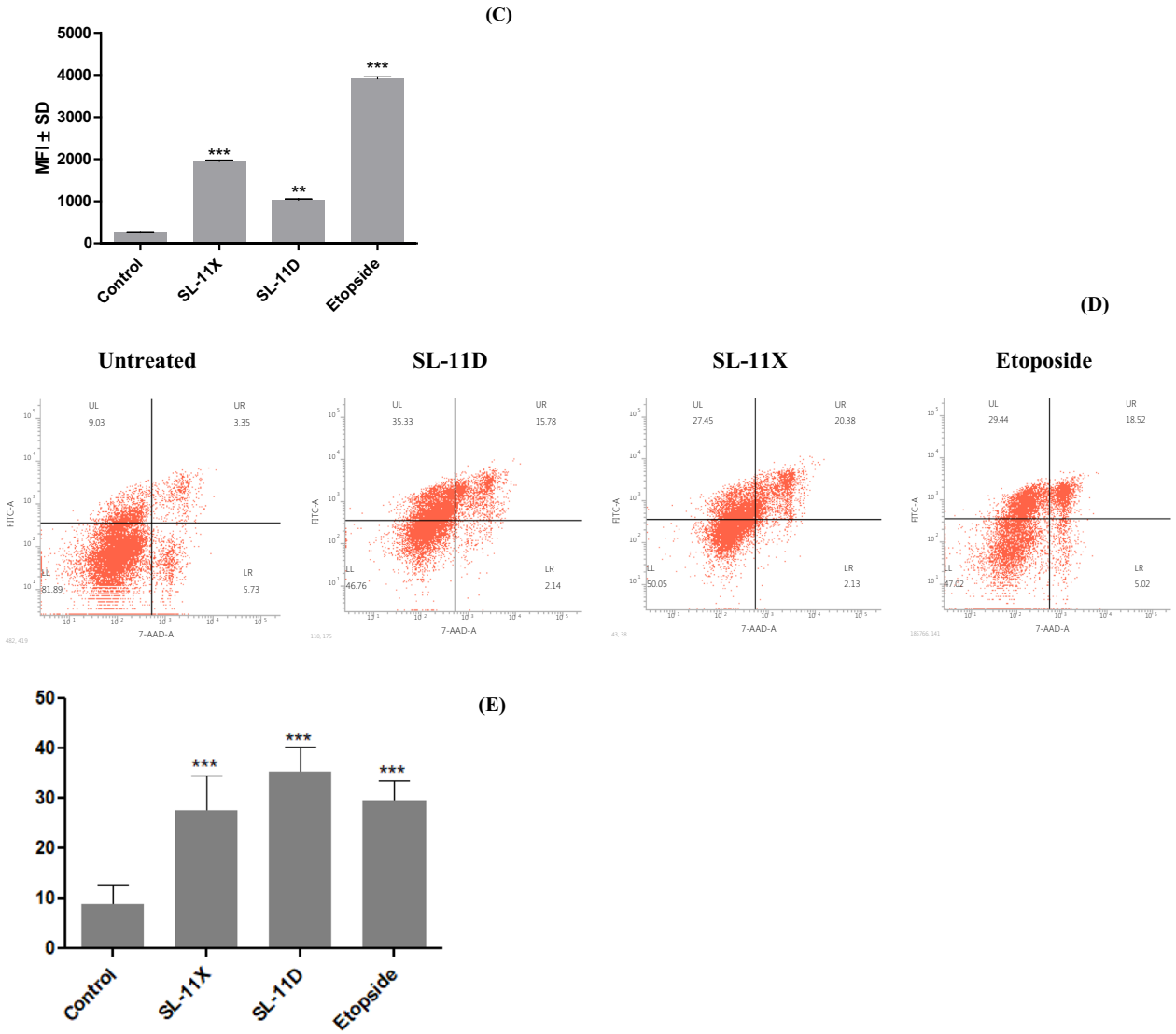

Fig. 6 continued

Effect of SL-11D and SL-11X on actin filaments

ZO1/phalloidin assay was used to determine the sophorolipids SL-11D and SL-11X effect on the actin filaments. A549 cells treated with SL-11D and SL-11X at a concentration of 50 µg/ml showed a loosening of actin filaments, whereas cells treated with DMSO showed a dense network of actin filaments (Fig. 6A). SL-11D and SL-11X were highly effective against A549 cancer cells. Glycolipids like sophorolipids are microbially derived biosurfactants with immunomodulatory and anticancer properties [58]. The actin filament network of A549 was also distorted by the addition of glucolipid and SL [8].

Effect of SL-11D and SL-11X on A549 cell line (live/dead staining)

Sophorolipid-treated samples were stained with acridine orange (AO) and ethidium bromide (EB) to detect apoptosis/necrosis. Cancer cells were treated with SL-11D and SL-11X for 24 h. Cancer cells treated with SL-11D and SL-11X appeared red, suggesting necrosed or dead cells. In the case of live and dead staining, acridine orange emits a green fluorescence and stains both living and dead cells when bound to the double helix. In contrast, ethidium bromide only stains the dead cells and transmits a red fluorescence (Fig. 6B). Most cells were red, but some had bright green spots, indicating cell necrosis.

SL-11D and SL-11X cause ROS production and necrosis in the A549 cancer cell line

FACS was used to evaluate the effect of SL-11D and SL-11X on ROS generation in A549 cancer cells. The results showed that both SL-11D and SL-11X, after 24 h of treatment, induced ROS production in cancer cells. In A549, 24.22% and 33.4% of the cells exhibited ROS generation after treatment with SL-11D and SL-11X, respectively (Fig. 6C). On the other hand, cells treated with etoposide (positive control) produced 46.66% of ROS, while untreated cells produced 2.49%.

Annexin/PI staining was used via FACS to observe the effect of sophorolipids on cancer cells. Approximately 35.3% and 27.4% of A549 cells treated with SL-11D and SL-11X exhibited necrosis. On the other hand, etoposide (positive control) showed 29.4% of cell necrosis, and untreated cells showed 9.03% of cell necrosis (Fig. 6D and E).

Phosphatidylserine (PS), a membrane phospholipid, is in transit from the inner to the outer leaflet of the plasma membrane during apoptosis. Positive signals are produced when annexin binds to exposed phosphatidylserine (PS) on the cell surface, indicating apoptotic activity. Conversely, propidium iodide (PI) only penetrates dead or damaged cells, being excluded by healthy or live cells. We observed that a significant proportion of the cell population appeared to be PI-positive, indicating necrosis in the cells. Numerous anticancer treatments may also result in tumor cell necrosis [59]. The results of our study demonstrated that ROS-dependent necrosis occurs in cancer cells. Some reports also suggested a potential role of kinase receptor-interacting protein (RIP1) in ROS-dependent necrosis. Haque et al. hypothesize that it might be possible that L-SL could induce ROS-dependent necrosis via activation of RIP1 and cause cell death in cancer cells [8]. In the present study, we speculate that SL-11D and SL-11X may cause ROS-dependent necrosis and cell death in cancer cells.

This study presents a newly discovered species within the *Metschnikowia* clade capable of producing sophorolipids, showcasing notable antimicrobial and anticancer properties. Ongoing research into yeast communities associated with insects continues to uncover additional species, opening avenues for harnessing their bioactive compounds in therapeutic applications [20]. Previous research has explored the antimicrobial effects of sophorolipids on certain gram-negative bacteria and pathogenic fungal species [3, 54, 60, 61]. To my understanding, this study marks the first exploration into the precise mechanisms through which sophorolipids exert their effects against *K. pneumoniae*, a gram-negative bacterium, and *F. solani*, a pathogen affecting plants and humans.

Future research should prioritize in-vivo studies using the *Klebsiella* mouse model to evaluate sophorolipids' effectiveness against infections. Additionally, investigating cancer models to assess sophorolipids' potential in treatment, exploring mechanisms of action, and optimizing formulations are crucial for clinical advancement.

Conclusion

This article contains two novel yeast species, *Metschnikowia dubei* f.a., sp. nov., CIG-11D^T, and *Metschnikowia shirgulensis* f.a, sp. nov., CIG-11X^T, which were isolated from a gut of bees. Significant yields of sophorolipids were obtained in bioreactors without using oil as a secondary source. This approach could potentially render the production process more cost-effective by eliminating expenses associated with secondary sources and downstream processing. Our study demonstrated sophorolipid's overall mechanism of action in disrupting bacterial and fungal membranes via ROS production supported by transmission electron microscopy, confocal microscopy, and ROS determination by FACS. The current study indicates that both sophorolipids can potentially regulate lung cancer cell growth via inducing apoptosis. ROS production may be the underlying mechanism for apoptosis. Therefore, both sophorolipids were chemo-preventive anti-tumor agents and could enhance anticancer therapies. Their efficacy underscores promising avenues for enhancing antibacterial, antifungal, and cancer treatment strategies. In addition to therapeutic applications, the current study demonstrates that sophorolipids exhibit robust stability under various physiological conditions. This suggests their potential utility in food formulations, microbial-enhanced oil recovery, and bioremediation efforts. Future research should prioritize the in-vivo mouse infection model studies to assess the effectiveness of sophorolipids against infections.

Supplementary Information

The online version contains supplementary material available at https://doi.org/10.1186/s12934-024-02489-9.

Supplementary Material 1.

Acknowledgements

SK and AK are thankful to the CSIR for the fellowship. We want to thank Dr. Neeraj Khatri for collecting blood samples, Mr. Kanhaya Lal for helping with the chemical structure of SL, and Dr. Nitish for providing standard. We acknowledge the home instrumentation facility's availability of instruments.

Author contributions

Sumeeta Kumari and Alka Kumari: Conceptualization, methodology, experimental work, writing, manuscript preparation. Asmita Dhiman: Cell Culture, confocal and FACS studies. Kanti Nandan Mihooliya: Process optimization and reactor studies and manuscript writing. Anil Kumar Pinnaka: Investigation, resource, review editing, and supervision. Manoj Raje: Resources and supervision in cell culture and confocal studies. G. S. Prasad: resources and supervision.

Funding
This study was funded by OLP-166 by Council of Scientific and Industrial Research (CSIR).

Availability of data and materials
This published article contains all the data analyzed in this study. The datasets presented in this study can be found in online depositories. Depositories: the strain has been deposited in NCBI under the accession number MG835365 (D1D2 domain of CIG-11D), and and MG835363 (D1/D2 domain of CIG-11X).

Declarations

Ethics approval and consent to participate
No ethical approval was required for insects, but the insect was euthanized using a method that caused minimum discomfort.

Competing interests
The authors declare no competing interests.

Author details
[1]Institute of Microbial Technology, CSIR, Sector 39-A, Chandigarh 160036, India.

Received: 10 June 2024 Accepted: 22 July 2024
Published online: 11 September 2024

References

1. Alberto N, Richard A, Thomas FA, Solaiman DKY. LC/MS analysis and lipase modification of the sophoroliids produced by *Rhodotorula bororiensis*. Biotechnol Lett. 2004;51:1087–93.
2. Kurtzman CP, Price NPJ, Ray KJ, Kuo TM. Production of sophorolipid biosurfactants by multiple species of the *Starmerella* (*Candida*) *bombicola* yeast clade. FEMS Microbiol Lett. 2010;311:140–6.
3. Sen S, Borah SN, Bora A, Deka S. Production, characterization, and antifungal activity of a biosurfactant produced by *Rhodotorula babjevae* YS3. Microb Cell Fact. 2017;16:1–14.
4. Santos DKF, Rufino RD, Luna JM, Santos VA, Salgueiro AA, Sarubbo LA. Synthesis and evaluation of biosurfactant produced by *Candida lipolytica* using animal fat and corn steep liquor. J Pet Sci Eng. 2013;105:43–50.
5. Ghasemi A, Moosavi-Nasab M, Setoodeh P, Mesbahi G, Yousefi G. Biosurfactant production by lactic acid bacterium *Pediococcus dextrinicus* SHU1593 grown on different carbon sources: strain screening followed by product characterization. Sci Rep. 2019;9:1–12.
6. Akiyode O, George D, Getti G, Boateng J. Systematic comparison of the functional physico-chemical characteristics and biocidal activity of microbial derived biosurfactants on blood-derived and breast cancer cells. J Colloid Interface Sci. 2016;479:221–33.
7. De Cesare GB, Cristy SA, Garsin DA, Lorenz MC. Antimicrobial peptides: a new frontier in antifungal therapy. MBio. 2020;11:1–21.
8. Haque F, Khan MSA, AlQurashi N. ROS-mediated necrosis by glycolipid biosurfactants on lung, breast, and skin melanoma cells. Front Oncol. 2021;11: 622470.
9. Pal S, Chatterjee N, Das AK, McClements DJ, Dhar P. Sophorolipids: a comprehensive review on properties and applications. Adv Colloid Interface Sci. 2023;313: 102856.
10. Gyanani V, Haley JC, Goswami R. Challenges of current anticancer treatment approaches with focus on liposomal drug delivery systems. Pharmaceuticals. 2021;14:835.
11. Nawale L, Dubey P, Chaudhari B, Sarkar D, Prabhune A. Anti-proliferative effect of novel primary cetyl alcohol derived sophorolipids against human cervical cancer cells HeLa. PLoS ONE. 2017;12: e0174241.
12. Rebecca Miceli T, David Corr T, Margarida Barroso M, Dogra N, Richard Gross A. Sophorolipids: anticancer activities and mechanisms. Bioorg Med Chem. 2022;65:116787.
13. Ribeiro IAC, Faustino CMC, Guerreiro PS, Frade RFM, Bronze MR, Castro MF, et al. Development of novel sophorolipids with improved cytotoxic activity toward MDA-MB-231 breast cancer cells. J Mol Recognit. 2015;28:155–65.
14. Rosa CA, Lachance MA, Silva JOC, Teixeira ACP, Marini MM, Antonini Y, et al. Yeast communities associated with stingless bees. FEMS Yeast Res. 2003;4:271–5.
15. De Vega C, Guzmán B, Steenhuisen SL, Johnson SD, Herrera CM, Marc-André L. *Metschnikowia drakensbergensis* sp. nov. and *Metschnikowia caudata* sp. nov., endemic yeasts associated with Protea flowers in South Africa. Int J Syst Evol Microbiol. 2014;64:3724–32.
16. Liu XJ, Cao WN, Ren YC et al. Taxonomy and physiological characterisation of Scheffersomyces titanussp. nov., a new D-xylose-fermenting yeast species from China. Sci Rep 2016;6:32181. https://doi.org/10.1038/srep32181.
17. Saluja P, Prasad GS. *Candida ruelliae* sp. nov., a novel yeast species isolated from flowers of *Ruellia* sp. (Acanthaceae). FEMS Yeast Res. 2008;8:660–6.
18. Kumari A, Mihooliya KN, Sahoo DK, Bhattacharyya MS, Prasad GS, Pinnaka AK. Description of lipase producing novel yeast species *Debaryomyces apis* f.a., sp. nov. and a modified pH indicator dye-based method for the screening of lipase producing microorganisms. Sci Rep. 2023;13:11819.
19. Kurtzman CP, Fell JW, Boekhout T, Robert V. Methods for isolation, phenotypic characterization and maintenance of yeasts. In: Kurtzman CP, Fell JW, Boekhout T, editors. The Yeasts (Fifth Edition), Elsevier, 2011. p. 87–110. https://doi.org/10.1016/B978-0-444-52149-1.00007-0
20. Kumari A, Kumari S, Prasad GS, Pinnaka AK. Production of sophorolipid biosurfactant by insect derived novel yeast *Metschnikowia churdharensis* f.a., sp. nov., and its antifungal activity against plant and human pathogens. Front Microbiol. 2021;12:6786.
21. Kimura M. A simple method for estimating evolutionary rates of base subsitution through comparative studies of nucleotides sequences. J Mol Evol. 1980;16:111–20.
22. Saitou N, Nei M. The neighbor-joining method : a new method for reconstructing phylogenetic trees'. Mol Biol Evol. 1987;4:406–25.
23. Kumar S, Stecher G, Tamura K. MEGA7: molecular evolutionary genetics analysis version 7.0 for bigger datasets. Mol Evol Genet Anal. 2016;33:1870–4.
24. Felsenstein J. Confidence limits on phylogenies: an approach using the bootstrap. Soc Study Evol. 1985;39:783–91.
25. Bonilla M, Olivaro C, Corona M, Vazquez A, Soubes M. Production and characterization of a new bioemulsifier from *Pseudomonas putida* ML2. J Appl Microbiol. 2005;98:456–63.
26. Abdel-Fattah YR, Olama ZA. L-asparaginase production by *Pseudomonas aeruginosa* in solid-state culture: evaluation and optimization of culture conditions using factorial designs. Process Biochem. 2002;38:115–22.
27. Mahajan RV, Saran S, Kameswaran K, Kumar V, Saxena RK. Efficient production of l-asparaginase from *Bacillus licheniformis* with low-glutaminase activity: optimization, scale up and acrylamide degradation studies. Bioresour Technol. 2012;125:11–6.
28. Mihooliya KN, Nitika N, Bhambure R, Rathore AS. Post-refolding stability considerations for optimization of in-vitro refolding: L-asparaginase as a case study. Biotechnol J. 2023;18:2200505.
29. Mihooliya KN, Nandal J, Kumari A, Nanda S, Verma H, Sahoo DK. Studies on efficient production of a novel l-asparaginase by a newly isolated *Pseudomonas resinovorans* IGS-131 and its heterologous expression in *Escherichia coli*. 3 Biotech. 2020;10:1–11.
30. Fontes GC, Ramos NM, Amaral PFF, Nele M, Coelho MAZ. Renewable resources for biosurfactant production by *Yarrowia lipolytica*. Braz J Chem Eng. 2012;29:483–93.
31. Camargo FP, de Menezes AJ, Tonello PS, Dos Santos ACA, Duarte ICS. Characterization of biosurfactant from yeast using residual soybean oil under acidic conditions and their use in metal removal processes. FEMS Microbiol Lett. 2018;365:1–8.
32. Santos DA, Hamdan JS. Evaluation of broth microdilution antifungal susceptibility testing conditions for *Trichophyton rubrum*. J Clin Microbiol. 2005;43:1917–20.
33. Baindara P, Chaudhry V, Mittal GG, Liao LM, Matos CO, Khatri N, et al. Characterization of the antimicrobial peptide penisin, a class ia novel lantibiotic from *Paenibacillus* sp. strain A3. Antimicrob Agents Chemother. 2016;60:1–12.
34. Malhotra H, Patidar A, Boradia VM, Kumar R, Nimbalkar RD, Kumar A, et al. *Mycobacterium tuberculosis* glyceraldehyde-3-phosphate dehydrogenase (GAPDH) functions as a receptor for human lactoferrin. Front Cell Infect Microbiol. 2017;7:245.

35. Haque F, Alfatah M, Ganesan K, Bhattacharyya MS. Inhibitory effect of sophorolipid on *Candida albicans* biofilm formation and hyphal growth. Sci Rep. 2016;6:1–11.
36. Liang CC, Park AY, Guan JL. In vitro scratch assay: a convenient and inexpensive method for analysis of cell migration in vitro. Nat Protoc. 2007;2:329–33.
37. Kasibhatla S, Amarante-Mendes GP, Finucane D, Brunner T, Bossy-Wetzel E, Green DR. Acridine orange/ethidium bromide (AO/EB) staining to detect apoptosis. CSH Protoc. 2006;2006:pdb.prot4493.
38. Rieger AM, Nelson KL, Konowalchuk JD, Barreda DR. Modified annexin V/propidium iodide apoptosis assay for accurate assessment of cell death. J Vis Exp. 2011;50: e2597.
39. Ali W, Alwaely S, Alrubayae I, Alwaely WAS, Ghadban AK, Alrubayae IMN. Production and properties of biosurfactant from the local isolation of *Candida* spp. Drug Invention Today. 2019;12:948–53.
40. Amaral PFF, Coelho MAZ, Marrucho IMJ, Coutinho JAP. Biosurfactants from yeasts: characteristics, production and application. Adv Exp Med Biol. 2010;672:236–49.
41. Elshafie AE, Joshi SJ, Al-Wahaibi YM, Al-Bemani AS, Al-Bahry SN, Al-Maqbali D, et al. Sophorolipids production by *Candida bombicola* ATCC 22214 and its potential application in microbial enhanced oil recovery. Front Microbiol. 2015;6:1–11.
42. Banat IM. Biosurfactants production and possible uses in microbial enhanced oil recovery and oil pollution remediation: a review. Bioresour Technol. 1995;51:1–12.
43. Santos DKF, Resende AHM, de Almeida DG, de Soares Silva RCF, Rufino RD, Luna JM, et al. *Candida lipolytica* UCP0988 biosurfactant: potential as a bioremediation agent and in formulating a commercial related product. Front Microbiol. 2017;8:1–11.
44. Sarubbo LA, Farias CBB, Campos-Takaki GM. Co-utilization of canola oil and glucose on the production of a surfactant by *Candida lipolytica*. Curr Microbiol. 2007;54:68–73.
45. Haaland PD. Experimental design in biotechnology. 1st ed. CRC Press; 1989. p. 1–59.
46. Daverey A, Pakshirajan K. Sophorolipids from *Candida bombicola* using mixed hydrophilic substrates: production, purification and characterization. Colloids Surf B Biointerfaces. 2010;79:246–53.
47. Daverey A, Pakshirajan K. Production, characterization, and properties of sophorolipids from the yeast *Candida bombicola* using a low-cost fermentative medium. Appl Biochem Biotechnol. 2009;158:663–74.
48. de Cortés-Sánchez AJ, Hernández-Sánchez H, Jaramillo-Flores ME. Biological activity of glycolipids produced by microorganisms: new trends and possible therapeutic alternatives. Microbiol Res. 2013;168:22–32.
49. Dengle-Pulate V, Joshi J, Bielefeld F, Bhagwat S, Prabhune A. Application of sophorolipid synthesized using lauryl alcohol as a germicide and fruit-vegetable wash. World J Pharm Pharm Sci. 2014;3:1630–43.
50. Hipólito A, Alves da Silva RA, de Caretta TO, Silveira VAI, Amador IR, Panagio LA, et al. Evaluation of the antifungal activity of sophorolipids from *Starmerella bombicola* against food spoilage fungi. Biocatal Agric Biotechnol. 2020;29: 101797.
51. Basak G, Das D, Das N. Dual role of acidic diacetate sophorolipid as biostabilizer for ZnO nanoparticle synthesis and biofunctionalizing agent against *Salmonella enterica* and *Candida albicans*. J Microbiol Biotechnol. 2014;24:87–96.
52. Kim SY, Park C, Jang HJ, Kim BO, Bae HW, Chung IY, et al. Antibacterial strategies inspired by the oxidative stress and response networks. J Microbiol. 2019;57:203–12.
53. Cho WY, Ng JF, Yap WH, Goh BH. Sophorolipids—bio-based antimicrobial formulating agents for applications in food and health. Molecules. 2022;27:5556.
54. Shikha S, Kumar V, Jain A, Dutta D, Bhattacharyya MS. Unraveling the mechanistic insights of sophorolipid-capped gold nanoparticle-induced cell death in *Vibrio cholerae*. Microbiol Spectr. 2023;11: e00175-23.
55. Görlach A, Bertram K, Hudecova S, Krizanova O. Calcium and ROS: a mutual interplay. Redox Biol. 2015;6:260–71.
56. Ribeiro BG, Guerra JMC, Sarubbo LA. Potential food application of a biosurfactant produced by *Saccharomyces cerevisiae* URM 6670. Front Bioeng Biotechnol. 2020;8:1–13.
57. Maeng Y, Kim KT, Zhou X, Jin L, Kim KS, Kim YH, et al. A novel microbial technique for producing high-quality sophorolipids from horse oil suitable for cosmetic applications. Microb Biotechnol. 2018;11:917–29.
58. Adu SA, Twigg MS, Naughton PJ, Marchant R, Banat IM. Biosurfactants as anticancer agents: glycolipids affect skin cells in a differential manner dependent on chemical structure. Pharmaceutics. 2022;14:360.
59. Proskuryakov S, Gabai V. Mechanisms of tumor cell necrosis. Curr Pharm Des. 2009;16:56–68.
60. Chen J, Liu X, Fu S, An Z, Feng Y, Wang R, et al. Effects of sophorolipids on fungal and oomycete pathogens in relation to pH solubility. J Appl Microbiol. 2020;128:1754–63.
61. da Fontoura ICC, Saikawa GIA, Silveira VAI, Pan NC, Amador IR, Baldo C, et al. Antibacterial activity of sophorolipids from *Candida bombicola* against human pathogens. Braz Arch Biol Technol. 2020;63: e20180568.

Publisher's Note